Mechanisms of Ageing and Development 228 (2025) 112116

Contents lists available at ScienceDirect

Mechanisms of Ageing and Development

journal homepage: www.elsevier.com/locate/mechagedev

Human astrocytes from healthy individuals and Alzheimer's patients respond differently to Aβ_{1-42} oligomers, triggering distinct paths of reactivity and senescence

Sara Ristori [a], Gianmarco Bertoni [a], Alessandra Bigi [a], Cristina Cecchi [a], Manuela Sollazzo [b], Luisa Iommarini [b], Daniela Monti [a,1,*], Elisa Bientinesi [a,1]

[a] Department of Experimental and Clinical Biomedical Sciences "Mario Serio", University of Florence, Florence 50134, Italy
[b] Department of Pharmacy and Biotechnology, University of Bologna, Bologna 40126, Italy

ARTICLE INFO

Keywords:
Alzheimer's disease
Astrocyte senescence
Aβ1–42 oligomers
Neuroinflammation
Reactive astrocytes

ABSTRACT

Alzheimer's disease (AD) is a neurodegenerative disorder characterised by cognitive decline, amyloid-β (Aβ) plaques, and neurofibrillary tangles. Aβ_{1-42} oligomers exert neurotoxic and pro-inflammatory effects. Astrocytes maintain brain homeostasis, and their dysfunction contributes to AD progression. This study investigates the impact of Aβ_{1-42} oligomers on primary human astrocytes from healthy individuals and AD patients. Our findings show that astrocytes from both groups internalise Aβ_{1-42} oligomers. In healthy astrocytes, internalisation enhances proteasome activity, whereas in AD astrocytes, it reduces it. Aβ_{1-42} oligomers induce calcium dyshomeostasis and mitochondrial membrane potential alterations in both groups. Interestingly, oligomers induce apoptosis in a subset of healthy astrocytes, while surviving ones become reactive and hyperproliferative, releasing neuroinflammatory and neurotrophic molecules. Conversely, Aβ_{1-42} drives AD astrocytes into senescence, characterised by increased β-galactosidase activity, p14^{ARF} expression, senescence-associated secretory phenotype (SASP), and heterochromatin foci. Importantly, conditioned media from Aβ_{1-42}-treated AD astrocytes, but not from healthy ones, cause death of differentiated SH-SY5Y neuron-like cells, suggesting that senescent astrocytes contribute to neurotoxicity. These findings reveal differential astrocytic responses to Aβ_{1-42} oligomers, emphasising the importance of astrocyte senescence in AD pathogenesis. This research offers insight into cellular mechanisms underlying AD and may support the development of innovative therapeutic strategies for neurodegenerative diseases.

Glossary

Aβ_{1-42} (Amyloid beta 1–42) A 42-amino acid peptide derived from the amyloid precursor protein (APP) via proteolytic cleavage, prone to aggregation and implicated in the pathogenesis of Alzheimer's disease.

Senescence associated β-galactosidase (SA-β-Gal) activity A biomarker used to detect cellular senescence through pH-dependent enzymatic activity observable by blue staining.

Clathrin-dependent endocytosis A cellular process for internalizing substances through clathrin-coated vesicles, often involved in the uptake of extracellular aggregates like Aβ.

Conditioned Medium (CM) Culture medium collected from treated and control cells containing secreted factors, used to assess paracrine effects on other cell types.

GFAP (Glial Fibrillary Acidic Protein) An astrocytes intermediate filament protein commonly used as a marker of astrocyte activation and reactive gliosis.

Ki-67 A nuclear protein expressed during active phases of the cell cycle, used as a marker of cellular proliferation.

MacroH2A.1 A histone variant associated with senescence-associated heterochromatin foci (SAHF), a hallmark of cellular senescence.

MMPs (Matrix Metalloproteinases) A family of zinc-dependent

* Corresponding author.
E-mail addresses: sara.ristori@unifi.it (S. Ristori), gianmarco.bertoni@unifi.it (G. Bertoni), alessandra.bigi@unifi.it (A. Bigi), cristina.cecchi@unifi.it (C. Cecchi), manuela.sollazzo2@unibo.it (M. Sollazzo), luisa.iommarini2@unibo.it (L. Iommarini), daniela.monti@unifi.it (D. Monti), elisa.bientinesi@unifi.it (E. Bientinesi).
[1] Co-last author

https://doi.org/10.1016/j.mad.2025.112116

Available online 24 September 2025

endopeptidases involved in extracellular matrix remodeling; often upregulated in neuroinflammation.

Neuroblastoma SH-SY5Y cells A human-derived neuronal cell line used as an *in vitro* model for neuronal function and differentiation.

Proteasome A multi-protein complex responsible for degrading misfolded or damaged proteins via the ubiquitin-proteasome system.

Quantibody Array A multiplexed sandwich ELISA-based assay used for the quantitative detection of multiple cytokines or growth factors in a single sample.

Reactive astrocytes Astrocytes that have undergone morphological and functional changes in response to injury or disease, often characterised by increased GFAP expression.

SASP (Senescence-Associated Secretory Phenotype) A pro-inflammatory and tissue-remodeling secretory profile developed by senescent cells, which can influence the surrounding microenvironment.

Senescence-associated heterochromatin foci (SAHF) Regions of condensed chromatin formed in senescent cells, marked by histone modifications such as macroH2A.1.

TIMP-1 (Tissue Inhibitor of Metalloproteinases-1) An endogenous inhibitor of metalloproteinases, involved in regulating ECM degradation and inflammation.

1. Introduction

Aging is a natural and universal feature of most living organisms that, in humans, has already become a medical and social priority due to the prevalence of elderly subjects in the population caused by increased life expectancy (Ostan et al., 2008). Unfortunately, the extensive modifications that accompany the aging process contribute to an increased risk of developing age-related diseases (ARDs), such as cardiovascular pathologies, cancer, and neurodegenerative disorders (Franceschi et al., 2018). Alzheimer's disease (AD) is the primary cause of dementia in aged people and poses an important challenge for current and future healthcare systems. Interestingly, women have a greater risk of developing dementia during their lifetime and also tend to have a worse prognosis and experience faster rates of cognitive decline than men (Alzheimer Association, 2020; Barnes et al., 2005; Koran et al., 2017; Ostan et al., 2016; Rabin et al., 2019). AD is characterised by brain atrophy, loss of neurons and synapses, neuroinflammation and the accumulation of two definitive pathological lesions: neurofibrillary tangles, composed of hyperphosphorylated Tau, and senile plaques, formed by the amyloid-β (Aβ) peptide (Barragán Martínez et al., 2019). Although significant progress has been made in understanding the molecular pathogenic events of AD in recent years, its underlying causes remain largely unknown, and no definitive curative treatments are currently available (Sheppard and Coleman, 2020). The dominant model of AD pathogenesis is the Aβ hypothesis, which proposes that the critical feature of AD is the presence of senile plaques in the brain, mainly formed by the misfolded and assembled Aβ, produced along the amyloidogenic pathway (Selkoe and Hardy, 2016). Amyloid plaques are extracellular deposits of Aβ, abundant in the cortex of AD patients. The sequential cleavage of the amyloid precursor protein (APP) by β- and γ-secretase produces a small fragment, which is more hydrophobic and consequently prone to fibrillation (Pannuzzo, 2022). The aggregation process of Aβ can produce different types of oligomers, protofibrils, and fibrils. Several studies demonstrated that the Aβ neurotoxic effects could be attributed to the soluble and diffuse oligomeric forms sufficient to induce neuronal cell death (Bigi et al., 2023; Chiti and Dobson, 2017; Kayed et al., 2003). However, although neuronal death has a significant correlation with AD onset and progression, other brain cell types may contribute to the development and prognosis of the disease. Among brain cells, astrocytes are the major glial cells, responsible for the complex and essential functions of the Central Nervous System (CNS), supporting the blood-brain barrier (BBB) and preserving the extracellular ion balance (Csipo et al., 2020; Han et al., 2020). Additionally, they are crucial in regulating neuron survival, metabolism and synaptic plasticity. They also facilitate the uptake and recycling of neurotransmitters, supporting the hypothesis that they could be involved in the pathogenesis and development of AD (Acosta et al., 2017; Farhy-Tselnicker and Allen, 2018; Palmer and Ousman, 2018). In response to injury or stress and depending on the context, astrocytes may undergo cellular senescence or enter reactive states collectively referred to as gliosis (Lazic et al., 2022).

Cellular senescence is one of several interconnected biological processes involved in aging and the development of ARDs (Franceschi and Campisi, 2014; He and Sharpless, 2017; López-Otín et al., 2022; Rodier and Campisi, 2011). It is defined as a permanent state of cell cycle arrest, characterised by altered gene expression, increased secretion of pro-inflammatory factors (senescence-associated secretory phenotype, SASP), resistance to apoptosis, and changes in cellular morphology (Cevenini et al., 2013; González-Gualda et al., 2021). Astrocytes are particularly susceptible to senescence, which can be triggered by stimuli, such as replicative exhaustion, oxidative stress, DNA damage, or proteostatic alterations (Matias et al., 2022; Shafqat et al., 2023; Turnquist et al., 2016). Senescent astrocytes exhibit canonical markers such as upregulation of $p16^{INK4a}$, $p14^{ARF}$ and p21, increased senescence-associated β-galactosidase (SA-β-Gal) activity, loss of lamin-B1, mitochondrial dysfunction and elevated ROS production, along with the SASP (Cohen and Torres, 2019; Han et al., 2020; Lye et al., 2019; Shafqat et al., 2023). These changes impair critical astrocytic functions, including glutamate uptake, neurotrophic support, and BBB regulation, thereby promoting excitotoxicity, neuroinflammation and neuronal dysfunction in aging and AD (Han et al., 2020; Shafqat et al., 2023; Tuzer and Torres, 2022). Recent evidence also suggests that accumulation of senescent astrocytes in AD-relevant brain regions may play a role in disease progression, making astrocyte senescence a promising therapeutic target for interventions aimed at SASP modulation or senolytic clearance (Bussian et al., 2018; Hudson et al., 2025).

Astrogliosis, on the other hand, is characterised by morphological changes, hyperproliferation, upregulation of intermediate filament proteins (such as GFAP and vimentin), transcriptional reprogramming, and secretion of inflammatory molecules (Pekny et al., 2014). Reactive astrocytes are commonly observed around Aβ plaques and are strongly associated with neuroinflammation (Habib et al., 2020). However, growing evidence suggests that astrogliosis is a highly heterogeneous and context-dependent process (Anderson et al., 2013). Importantly, reactive astrocytes can also exert beneficial functions, such as promoting synaptic support, maintaining blood–brain barrier integrity, modulating inflammation, and facilitating tissue repair (Escartin et al., 2021; Pekny and Pekna, 2014; Sofroniew, 2015). In this study, we investigated how oligomers formed by the 42-residue form of Aβ peptide ($Aβ_{1–42}$) affect human primary astrocytes derived from both healthy individuals and AD patients. Our goal was to explore any differences in their responses to treatment and clarify the pathogenetic mechanisms underlying the disease. We specifically examined the internalisation of $Aβ_{1–42}$ oligomers, their impact on proteasomal activity and calcium homeostasis, and their effects on key cellular processes, such as apoptosis, senescence, and astrocyte reactivity. Additionally, we evaluated the effects of conditioned medium from treated healthy and AD astrocytes on differentiated neuroblastoma cells to assess their neurotoxicity.

2. Materials and methods

2.1. Reagents

Lyophilised Amyloid β-Protein (1−42) ($Aβ_{1–42}$) (#4014447; Bachem AG, Switzerland) was dissolved in 1,1,1,3,3,3-Hexafluoro-2-propanol (HFIP) (Sigma-Aldrich, St. Louis, MO, USA) to obtain monomers at a concentration of 1 mM and stored at −20°C until use. Dynasore hydrate (#D7693; Sigma-Aldrich, St. Louis, MO, USA) was dissolved in dimethyl

sulfoxide (DMSO) (#D8418; Sigma-Aldrich, St. Louis, MO, USA) to a stock concentration of 10 mg/mL and stored at −20°C until use. Carbonyl cyanide 4-(trifluoromethoxy)phenylhydrazone (FCCP) (#C2920; Sigma-Aldrich, St. Louis, MO, USA) was dissolved in DMSO to a concentration of 12 mM and stored at −20°C until use. The retinoic acid (RA) (#R2625; Sigma-Aldrich, St. Louis, MO, USA) was dissolved in DMSO to a stock concentration of 100 mM and stored at −20°C until use. RA was added to the cell culture medium at the final selected concentration. 5-Bromo-4 Chloro-3-Indolyl B-D-*Galactop B4252 was purchased from Sigma-Aldrich.

2.2. Cell lines and culture conditions

Authenticated human primary astrocytes (#36058–01 Celprogen Inc., Torrance, CA, USA) were obateined from six healthy donors (4 females, lot #1514431, #1514413, #1514423, #1514438 and 2 males, lot #1514449, #1514420, with a mean age of 49 ± 4.9 years, age range: 33–65 years) and five AD patients (2 females, lot #20274, #20262, and 3 males, lot #20255, #20256, #20260, with a mean age 83 ± 5.6 years, age range: 73–88 years). Cells were grown in complete Dulbecco's Modified Eagle Medium (DMEM) supplemented with 10 % heat-inactivated fetal bovine serum (FBS), 100 U/mL penicillin, 100 μg/mL streptomycin, 0.25 μg/mL amphotericin B, and 2 mM L-glutamine, and maintained at 37°C in a 5 % CO_2 humidified incubator. We used cells with a population doubling level < 30 to avoid replicative senescence.

Authenticated neuroblastoma SH-SY5Y cells (ATCC, Manassas, VA, USA) were cultured in complete neuroblastoma medium (DMEM HIGH/F-12 Ham 1:1, supplemented with 10 % of heat-inactivated FBS, 100 U/mL Penicillin, 100 μg/mL Streptomycin, 0.25 μg/mL Amphotericin B, and 2 mM L-Glutamine) at 37°C in 5 % CO2 humidified incubator. Before all experiments, SH-SY5Y were differentiated with retinoic acid (RA) for one week (Kovalevich and Langford, 2013). Briefly, an adequate number of SH-SY5Y cells (10.6 $\times 10^3$ cells/cm2) were plated in complete neuroblastoma medium, and after 24 h, the medium was exchanged with the differentiation medium (DMEM HIGH/F-12 Ham 1:1, supplemented with 1 % of heat-inactivated FBS, 100 U/mL Penicillin, 100 μg/mL Streptomycin, 0.25 μg/mL Amphotericin B, 2 mM L-Glutamine plus 10 μM RA). The differentiation medium was replaced every two days for a week. The acquisition of neuron-like phenotype was confirmed by morphological changes and increased expression of the neuronal marker β3-tubulin, as assessed by immunofluorescence.

2.3. Preparation of $A\beta_{1–42}$ oligomers and astrocyte treatment

Amyloid β-Protein (1−42) (#4014447; Bachem, Bubendorf, Switzerland) was prepared and oligomerised according to established protocols commonly used in the literature, in which the oligomeric state and purity of the preparation were validated by Western blotting and atomic force microscopy (AFM) (Bhat et al., 2012; Stine et al., 2003). Briefly, the lyophilised peptide was dissolved in 1,1,1,3,3,3,-hexafluoro-2-propanol (HFP) (#105228, Sigma-Aldrich, St. Louis, MO, USA) to 1 mM concentration to obtain monomers, aliquoted, and stocked at −20°C until use. In order to generate oligomeric $A\beta_{1–42}$, the solvent was evaporated, and the peptide film was resuspended in dimethyl sulfoxide (DMSO; D8418, Sigma-Aldrich, St. Louis, MO, USA) at 5 mM, sonicated for 10 min in the ultrasonic bath sonicator (USC100T, Avantor®, VWR International, Radnor, Pennsylvania, USA). The suspension was then diluted in complete culture medium supplemented with 2 % (v/v) FBS to a final concentration of 10 μM (monomer equivalents) and incubated at 4°C for 24 h. Before the experiments, an adequate number of human primary astrocytes (5.3 $\times 10^3$ cells/cm^2) were plated for 24 h in complete culture medium. Subsequently, the complete medium was removed, and cells were treated with $A\beta_{1–42}$ oligomers, prepared as previously described, for different times.

2.4. Confocal microscopy analysis for the internalisation of $A\beta_{1–42}$ oligomers

Human primary astrocytes were plated on sterile coverslips in 12-well plates and treated with $A\beta_{1–42}$ oligomers for 1, 24, 48, 72 and 120 h. In another set of experiments, astrocytes were pre-treated with dynamin inhibitor I, dynasore 80 μM, for 30 min at 37°C. Then, cells were treated with $A\beta_{1–42}$ oligomers with or without dynasore for 48 h at 37°C, replenishing dynasore every 24 h. After each time point, cells were washed with PBS and labelled with Alexa Fluor 633-conjugated wheat germ agglutinin (W21404, Thermo Fisher Scientific) (5.0 μg/mL) for 15 min at 37 °C. Afterwards, samples were fixed with 4 % (v/v) paraformaldehyde, permeabilised with 0.1 % Triton X-100 for 5 min, quenched with sodium borohydride, and washed. To detect the presence of oligomers, slides were incubated at RT for three hours with PBS-1 % FBS-diluted primary antibody (mouse monoclonal 6E10 anti-Aβ antibodies, BioLegend, CA, USA). Subsequently, slides were washed three times and incubated for 1 h at 37°C with Alexa Fluor 488-conjugated anti-mouse secondary antibody (Life Technologies, CA, USA). Fluorescence emission was detected upon sequential excitation at 488 nm and 633 nm by the TCS SP8 scanning confocal microscopy system (Leica Microsystems, Mannheim, Germany) equipped with an argon laser source. A series of 1.0-μm-thick optical sections (1024 × 1024 pixels) was taken through the cell depth for each sample using a Leica Plan Apo × 63 oil immersion objective. Apical, median and basal sections were projected as a single composite image by superimposition. ImageJ software (rsb.info.nih.gov) was used for immunofluorescence analysis. Aβ green fluorescence was measured inside the cells in the basal and median planes to quantify internalisation, while fluorescence in the apical plane was considered extracellular.

In a set of experiments, collected images were de-convolved with Huygens Professional software (Scientific Volume Imaging B.V., Hilversum, The Netherlands; version 18.04) and analysed with Leica Application Suite X (LAS-X) software (Leica) to generate 3D reconstructions, as reported previously (Bigi et al., 2020).

2.5. Proteasome activity

The proteasomal activity was assessed by using a Proteasome Activity Assay kit (ab107921, Abcam) following the manufacturer's protocol. After 48 and 120 h of $A\beta_{1–42}$ oligomers treatment, astrocytes were lysed in ice-cold PBS containing 0.5 % NP-40 and the supernatant was collected. Protein concentration was determined using the Pierce™ BCA Protein assay kit (#23225 ThermoFisher Scientific, Waltham, MA, USA), and 10 μg of protein from each sample was added to a 96-well fluorescent compatible plate with or without a proteasome inhibitor (provided with the kit). The plate was incubated at 37°C for 20 min, protected from light and then read with excitation of 350 nm and emission of 440 nm every 5 min for 60 min using a SYNERGY H1 microplate reader. The standard curve was generated using different concentrations of a 7-amino-4-methylcoumarin-(AMC)-tagged peptide that releases highly fluorescent AMC when exposed to proteolytic activity. The change in relative fluorescence units (RFUs) between the 50 and 20-minute points was plotted on the standard curve to determine AMC levels in the sample wells generated specifically by the proteolytic activity. The proteasome activity rate was determined by dividing the amount of fluorescent AMC by the difference between the two time points, multiplied by the volume of sample added into each reaction well (pmol AMC/min×μl).

2.6. Intracellular calcium evaluation

Intracellular calcium levels were evaluated by confocal microscopy and cytofluorimetric analyses. For confocal imaging, human primary astrocytes were plated in 12-well plates, treated with $A\beta_{1–42}$ oligomers for different time points, and loaded with 5 μM Fluo-4 AM (#F14201 ThermoFisher Scientific, Waltham, MA, USA) for 30 min at 37°C. Cells

were then washed and maintained in PBS for live imaging. Fluorescence was acquired using the Leica SP8 TCS confocal microscopy equipped with a 488 nm excitation laser. For cytofluorimetric analysis, treated cells were labelled with the probe Fluo-4 AM 5 μM diluted in medium with or without Ca^{2+} (Gibco, #21068028, ThermoFisher Scientific, Waltham, MA, USA) for 30 min at 37°C in the dark. Cells were then detached with trypsin with or without EDTA, washed twice in PBS, and resuspended in fresh medium before FACS analysis. After excitation at 488 nm, the analysis was carried out via BD FACS CANTO II and BD FACSDIVA software. Subsequently, raw data were evaluated using FlowJo software (Becton, Dickinson (BD) and & Company, Franklin Lakes, NJ, USA). Fluorescence intensities were expressed as the percentage relative to untreated cells.

2.7. MTT assay

Cell viability was determined by 3-(4,5-dimetiltiazol-2-il)-2,5-difeniltetrazolio (MTT) assay. In brief, human primary astrocytes and SH-SY5Y cells were seeded at an initial density of 2×10^3 and 6×10^3 cells/well, respectively, into 96-well plates and subjected to treatments described above. After 48 and 72 h of treatment for astrocytes and 24 h for SH-SY5Y cells, 80 μL of MTT solution (5 mg/mL) was added to each well and incubated for 4 h. Then, the supernatant was discarded, and 200 μL of HCl-Isopropanol solution was added to solubilise the formazan precipitates. The absorbance at 595 nm was read using a microplate reader. Cell viability was calculated as the ratio between untreated and treated cells' absorbance x 100 %.

2.8. Apoptosis evaluation by cytofluorimetric analysis

Cell death was evaluated using Annexin V Binding Buffer 10X (#556454), BV421 Annexin V (#563973), and 7AAD (#559925; all from Becton, Dickinson and & Company, Franklin Lakes, NJ, USA), after 48 and 72 h of treatment. Briefly, detached cells were incubated in FACS tubes with a working solution (Binding Buffer 1X, BV421 Annexin V, and 7-AAD) for 15 min at room temperature in the dark. Subsequently, cells were analysed with FACS CANTO II, and BD FACSDIVA software and data were evaluated using FlowJo Software (Becton, Dickinson and & Company, Franklin Lakes, NJ, USA). Cells that resulted positive only for Annexin V staining were considered early apoptotic, cells positive for both Annexin V and 7-AAD were considered in late apoptosis state and cells positive only for 7-AAD staining were considered necrotic. The cells negative for each staining were considered alive.

2.9. Measurement of Caspase 3–7 activity

Caspase 3–7 activity was evaluated using Caspase-Glo® 3/7 kit (#G8090, Promega, Madison, WI, USA), following the manufacturer's instructions. The assay provides a luminogenic caspase-3/7 substrate containing the tetrapeptide sequence DEVD in a reagent optimised for detecting caspase activity. The Caspase-Glo® 3/7 Reagent contains a proprietary thermostable luciferase (Ultra-Glo™ Recombinant Luciferase), which is formulated to generate a stable "glow-type" luminescent signal and improves performance across a wide range of assay conditions. Human primary astrocytes were seeded into 96-well plates, as described in the previous section and treated with $A\beta_{1-42}$ oligomers for 48 and 72 h. After treatment, the reagent was added to each well for 3 h at RT. The luminescent intensity was detected by SYNERGY H1 microplate reader. The luminescence intensities were expressed as the percentage of that measured in control cells.

2.10. Determination of mitochondrial membrane potential (ΔΨm)

The mitochondrial membrane potential (ΔΨm) was determined using the lipophilic probe 5,5′,6,6′-tertachloro-1,1′,3,3′-tetraethylbenzimidazol-carbocyanine iodide (JC-1, #420200, Sigma-Aldrich, St. Louis, MO, USA). The dye selectively accumulates in mitochondria, where its fluorescence emission changes based on ΔΨm. JC-1 aggregates and emits red fluorescence (590 nm) in the presence of high mitochondrial membrane potential, while at low membrane potential, it remains in monomeric form, emitting green fluorescence (530 nm). The red-to-green fluorescence intensity ratio indicates mitochondrial health, with a higher ratio reflecting intact ΔΨm and a lower ratio indicating depolarisation (Cossarizza et al., 1993; Salvioli et al., 1997). In this set of experiments, human primary astrocytes were plated on μ-Slide 8 Well high chamber (#80.826, Ibidi GmbH, Martinsried, Germany) (5.5×10^3 cells/cm^2) and treated with $A\beta_{1-42}$ as previously described. After 48, 72, and 120 h of treatment, cells were washed and incubated for 15 min at 37°C with JC-1 (5 μg/mL) and Hoechst (#33342, ThermoFisher Scientific, Waltham, MA, USA), diluted 1:1000, for nuclear staining in complete culture medium supplemented with 2 % FBS. Thereafter, the cells were washed twice, and the experiment was started. For positive control, carbonyl cyanide *p*-trifluoro-methoxyphenylhydrazone (FCCP) 50 μM was added to culture medium to uncouple mitochondria after JC-1 labelling. Dual-channel images were obtained on the TCS SP8 scanning confocal microscopy system described above after double excitation at 488 and 514 nm. ImageJ software (National Institutes of Health, Bethesda, MA, USA) was used for red and green fluorescence analysis. The red-to-green fluorescence intensity ratio was used to monitor changes in ΔΨm.

2.11. Senescence-associated β-galactosidase staining

Staining for SA-β-Gal was performed as described previously (Dimri et al., 1995). Human primary astrocytes were plated at 5.3×10^3 cells/cm^2 and assessed for SA-β-Gal activity after five days of $A\beta_{1-42}$ treatment. At least 300 cells *per* group were counted. Positive (blue) cells were expressed as a percentage of the total cell number.

2.12. Western blotting

The whole-cell lysate was obtained using Laemmli buffer, while the nuclear-cytoplasmic fractions were obtained using NE-PER™ Nuclear and Cytoplasmic Extraction Reagents (ThermoFisher Scientific, Waltham, MA, USA), following the manufacturer's instructions. Protein concentration was determined using the BCA Protein assay kit (ThermoFisher Scientific, Waltham, MA, USA). 50 μg of protein *per* sample were subjected to sodium dodecyl sulfate-polyacrylamide gel electrophoresis (SDS-PAGE) and blotted to a nitrocellulose membrane (Amersham Protran, GE Healthcare Life Science) by electroblotting. After blocking with bovine serum albumin (BSA) 5 %, the membrane was incubated with primary antibody against $p14^{ARF}$ (#74560, Cell Signaling Technology) and α-tubulin (sc-32293, Santa Cruz Biotechnology) at 4°C overnight. Washed membranes were incubated with IRDye800CW–conjugated or IRDye680–conjugated secondary antibody (LI-COR Biosciences, Lincoln, NE, USA) for one hour at room temperature. Antibody-coated bands were visualised by Odyssey Infrared Imaging System Densitometry (LI-COR Biosciences, Lincoln, NE, USA).

2.13. Immunostaining

Astrocytes were plated on sterile coverslips placed in 12-well plates, and the treatment was performed as described above. At the end of the experiments, cells were fixed in paraformaldehyde 4 % for 10 min at room temperature, permeabilised with 0.2 % Triton X-100 for 5 min, quenched with sodium borohydride, washed, and blocked for one hour with 1 % BSA 10 % horse serum at room temperature. Slides were incubated overnight at 4°C with primary antibodies in BSA 1 % (Histone Macro H2A.1, ABE215, Merck Millipore; γH2AX, #9718, Cell Signaling Technology; GFAP, #ab68428, Abcam; Vimentin, #5741, Cell Signaling Technology; Ki-67, #9129, Cell Signaling Technology). Slides were washed three times and incubated at room temperature for 40 min with

Alexa Fluor 488- or 633-conjugated secondary antibodies (goat anti-rabbit and goat anti-mouse, respectively, IgG (H+L) Cross-Adsorbed Secondary Antibody, ThermoFisher Scientific, Waltham, MA, USA). Nuclear DNA was stained with ProLong™ Gold Antifade Mountant with DAPI (ThermoFisher Scientific, Waltham, MA, USA). In another set of experiments, differentiated and undifferentiated SH-SY5Y were plated on sterile coverslips placed in 12-well plates and maintained for 24 h. Then, immunofluorescence was performed as described above, using β3 Tubulin (sc-80005, Santa Cruz Biotechnology) as the primary antibody. Slides were then visualised using the TCS SP8 scanning confocal microscopy system, Leica SP8 Confocal Microscope described above. ImageJ software (National Institutes of Health, Bethesda, MA, USA) was used for immunofluorescence analysis.

2.14. Quantibody array

Quantibody array was performed after 120 h of $A\beta_{1-42}$ treatment on human primary astrocytes with Quantibody Human Neuro Discovery Array 1 (RayBiotech, Norcross, GA, USA) following the manufacturer's instructions. The detected molecules are listed in Table 1. RayBiotech performed data extraction with microarray analysis software, and the data obtained was analysed using the Q-Analyzer software. To perform score analysis, molecule concentrations (pg/mL) were first normalised to their respective untreated control samples for each experimental group. Normalised values were then $\log_2$-transformed to obtain fold changes relative to control. For each sample, cumulative scores were calculated by summing the $\log_2$-transformed values of single molecules grouped into three functional categories: pro-inflammatory (IL-6, IL-8, IL-1α, TNFα, IFNγ, GM-CSF, MCP-1, Eotaxin, Eotaxin-2, MMP-2, and MMP-3), anti-inflammatory (IL-10, IL-4, and TGFβ1), and neurotrophic factors (BDNF, GDNF, β-NGF, CNTF, and EGF). This approach allowed a quantitative comparison of the overall molecular response within each category between HS and AD astrocytes following $A\beta_{1-42}$ treatment.

2.15. SH-SY5Y differentiation and treatment with conditioned media from astrocytes

Human primary astrocytes were treated with $A\beta_{1-42}$ oligomers, prepared as described above, for 120 h. At the end of treatment, the medium was removed, and the cells were washed and incubated for 24 h with fresh complete medium. The astrocyte-conditioned medium (CM) was collected, centrifuged and frozen at −80°C. Before all experiments, SH-SY5Y were differentiated with retinoic acid (RA) for seven days as described in paragraph 2.2. Subsequently, differentiated SH-SY5Y were treated with CM for 24 h, and viability and cell death were evaluated.

2.16. Statistical analysis

Statistical analysis was performed using GraphPad Prism 6.0 (GraphPad Software Inc., La Jolla, CA, USA). Data are expressed as the mean ± standard deviation (SD) of at least three independent experiments. P values were calculated using Student's *t*-test or one-way analysis of variance (ANOVA) followed by Tukey's post hoc test. Statistical significance was set at $p < 0.05$. To generate composite indices of cellular senescence and astrogliosis, z-scores were calculated for each marker across all treated samples and then averaged using the formula $z = (x - \mu) / \sigma$ where x is the individual value, μ is the mean, and σ is the standard deviation of the variable across all treated samples. These composite indices were used as dependent variables in multiple linear regression analyses (OriginPro 2024, OriginLab Corporation, Northampton, MA, USA). Regressions included only treated samples to isolate the effects of age (continuous, in years) and condition (categorical: 0 = healthy, 1 = AD), with degrees of freedom calculated as $df = n - k - 1 = 8$. For each predictor, unstandardised coefficients (β), standard errors (SE), t-values, and p-values were reported. 95 % confidence intervals were manually computed as $\beta \pm 2.306 \cdot SE$. Model fit was assessed via R^2 and adjusted R^2, and overall significance was tested using ANOVA (F-statistic and p-value). Significance was set at $p < 0.05$.

Table 1
Cytokines detected by Quantibody array.

IL-6	IL-8	IL-1α	BDNF	GDNF
IFNγ	TNFα	MMP−2	MMP−3	GM-CSF
MCP−1	Eotaxin	Eotaxin−2	β-NGF	EGF
CTNF	TGFβ1	TIMP−1	IL−10	IL−4

3. Results

3.1. Internalisation of $A\beta_{1-42}$ oligomers in astrocytes and their effect on proteasome activity

To gain deeper insights into the role of astrocytes in AD pathogenesis, we used astrocytes from healthy subjects (HS) and AD patients (AD) to assess their response to stress induced by $A\beta_{1-42}$ oligomers. We initially evaluated the ability of $A\beta_{1-42}$ oligomers (10 μM monomer equivalent) to interact and be taken up in the astrocyte cytosol after 1, 24, 48, 72, and 120 h of treatment. The plasma membranes (red) and oligomers (green) were counterstained and subsequently acquired at the apical, median and basal planes parallel to the coverslip using confocal scanning microscopy to evaluate $A\beta_{1-42}$ oligomers internalisation (Fig. 1a). $A\beta_{1-42}$ species entered both HS and AD astrocytes, as confirmed by the z-stack analysis used to perform the 3D reconstruction of the analysed cells, resulting in a pronounced green fluorescent signal within both cell types, as indicated by yellow arrows (Fig. 1b). Notably, an extracellular accumulation of $A\beta_{1-42}$ oligomers was evident in HS astrocytes, as indicated by blue arrows (Fig. 1b). The semi-quantitative analysis of the oligomer-derived fluorescence signal confirmed a significant intracellular increase in both astrocytes from HS and AD at all time points compared to untreated cells, which we refer to as control (100 %; Fig. 1c). Notably, sex-specific differences were observed in the internalisation of $A\beta_{1-42}$ oligomers by astrocytes (Fig. 1d). Specifically, astrocytes from female AD (F-AD) displayed significantly higher oligomer internalisation than those from male AD (M-AD). This difference was particularly pronounced at 72 h, where F-AD astrocytes also showed significantly higher internalisation than astrocytes from female HS (F-HS). Given the exploratory nature of sex-related analysis and the limited sample size for each sex subgroup, we report sex-based comparisons only when statistically supported. This approach was adopted to avoid overinterpretation of potentially spurious trends in underpowered subgroup analysis.

We then investigated one of the potential mechanisms through which astrocytes might internalise oligomers. To this aim, we inhibited the endocytotic process by pharmacological treatment with dynasore, dynamin inhibitor I, which evoked a significant inhibitory effect on oligomer entry, diminishing it by ~ 50 % (Fig. 2). The partial inhibition of the uptake suggests that, in addition to endocytosis, other mechanisms contribute to oligomer internalisation, allowing them to accumulate in the cytoplasm (Fig. 2a–b). Interestingly, when stratifying the samples by sex, dynasore reduced oligomer uptake more effectively in female astrocytes, both F-AD and F-HS, compared to male astrocytes (Fig. 2c). However, even after dynasore treatment, female astrocytes still had significantly more internalised $A\beta_{1-42}$ compared to male astrocytes. This suggests that, although dynasore does reduce uptake, female astrocytes may naturally take in more oligomers overall—even when endocytosis is blocked. So, the lower apparent effectiveness of dynasore in females may not mean they are less responsive to the drug. Instead, it could reflect their naturally higher baseline uptake. In this case, the percentage of reduction might be similar between sexes, but because females start from a higher level, the total amount of internalised oligomers remains higher in females.

We then examined the intracellular fate of internalised oligomers,

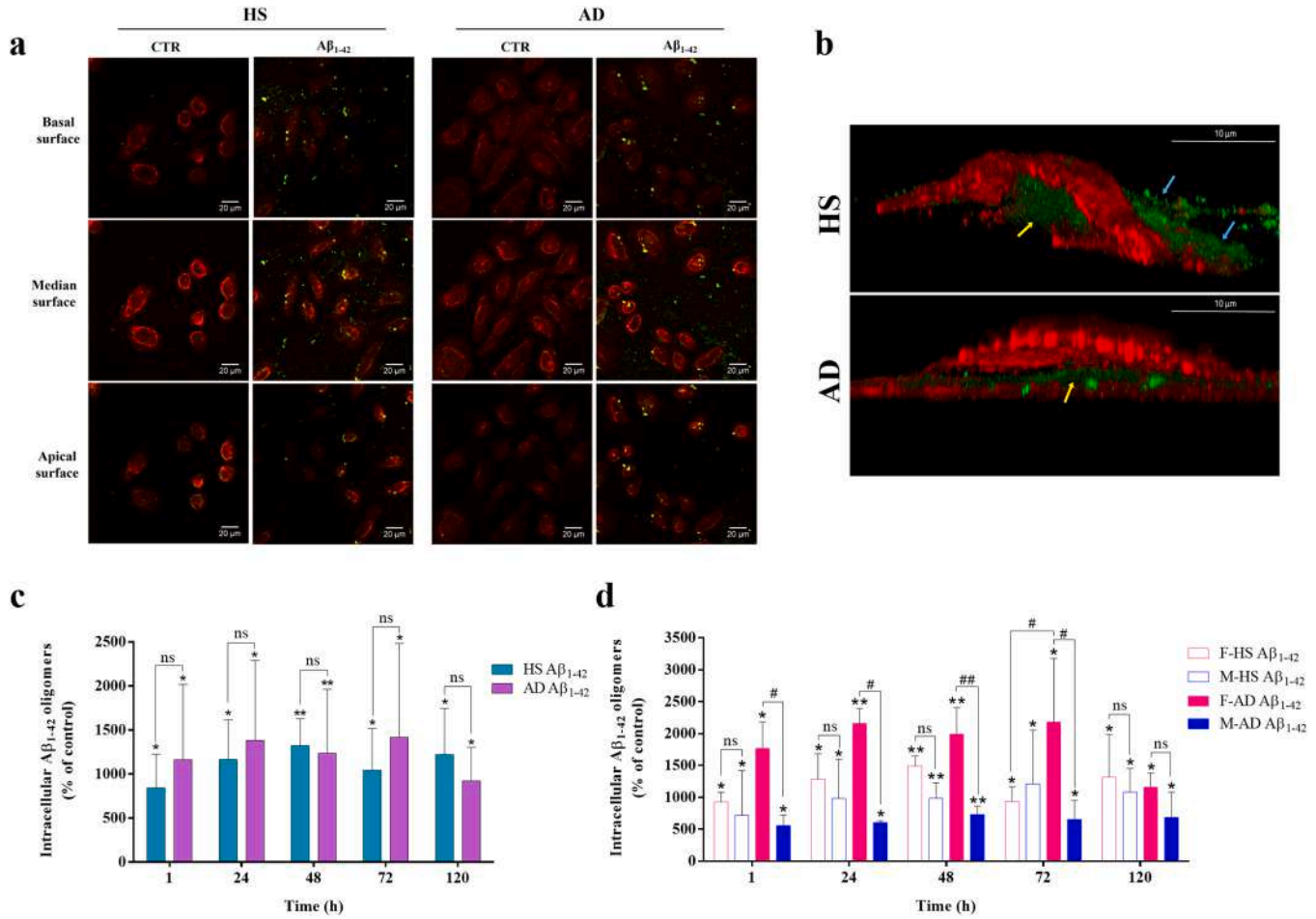

Fig. 1. $A\beta_{1-42}$ oligomers uptake in human primary astrocytes from healthy subjects and AD patients. (a) Representative confocal scanning microscope images at 48 h of treatment showing the basal, median and apical sections of control and treated astrocytes. Scale bars: 20 μm. (b) 3D reconstruction of the z-stack analysis at 48 h of treatment. Blue and yellow arrows indicate extracellular and intracellular oligomers, respectively. Scale bars: 10 μm. (c) Semi-quantitative analysis of the $A\beta_{1-42}$-derived fluorescence expressed as the percentage of endogenous $A\beta_{1-42}$ fluorescence in astrocytes from healthy subjects and AD patients treated for 1, 24, 48, 72, and 120 h with $A\beta_{1-42}$ oligomers. Data are expressed as the mean ± SD of two independent experiments. (d) The graph illustrates the percentage of endogenous $A\beta_{1-42}$ fluorescence in treated astrocytes from healthy subjects and AD patients, stratified by sex. Data are expressed as the mean ± SD of two independent experiments. Statistical significance is indicated as follows: * $p < 0.05$ and ** $p < 0.001$ vs control (set to 100 %); # $p < 0.05$ and ## $p < 0.001$ for comparisons between treated cells; ns: not significant. Abbreviations: CTR: control (untreated cells); HS: astrocytes from healthy subjects; AD: astrocytes from Alzheimer's patients; F-HS: astrocytes from female healthy subjects; M-HS: astrocytes from male healthy subjects; F-AD: astrocytes from female Alzheimer's patients; M-AD: astrocytes from male Alzheimer's patients.

specifically focusing on the mechanisms facilitating their degradation. Given the involvement of the 20S proteasome in the degradation of misfolded proteins, we assessed the proteasome activity after 48 and 120 h of treatment. Proteasome activity was significantly increased in treated astrocytes from HS at both times compared to controls, whereas AD astrocytes exhibited reduced activity (Fig. 3a). The representative RFU curve displayed at 48 h (Fig. 3b) further supports these findings. It shows that in treated HS astrocytes, proteasomal activity remains consistently higher than that of the control throughout the 60-minute time course, indicating a sustained increase in proteasomal function. In contrast, AD astrocytes exhibit lower RFU values during the assessment, with the treated group maintaining significantly lower activity than controls.

3.2. *$A\beta_{1-42}$ oligomers induce calcium dyshomeostasis, apoptosis, and mitochondrial depolarisation*

Some studies have demonstrated that Aβ oligomers, aberrantly interacting with astrocytes, are capable of inducing calcium dyshomeostasis within these cells, primarily through the release from intracellular stores. Thus, given the observed uptake of oligomers by our cells, we initially investigated the alterations in intracellular Ca^{2+} levels, using confocal microscopy to monitor time-dependent changes. Based on these preliminary results, no variations were observed at 1, 24, and 120 h of treatment compared to untreated cells (Supplementary Figure 1). In contrast, the two time points showing prominent results (48 and 72 h) were further analysed by flow cytometry, which confirmed a significant increase in intracellular calcium levels in both HS and AD treated astrocytes (Fig. 4a-b). To further investigate whether the changes in calcium concentrations were due to influx from the extracellular space or release from intracellular stores, astrocytes were incubated during the test in a calcium-free medium. At 48 and 72 h of treatment, the results indicated that the increase in intracellular calcium was primarily due to the release from intracellular reservoirs rather than influx from the extracellular space in both AD and HS astrocytes, as no significant differences were detected between the samples (Fig. 4c-d). Since elevated intracellular calcium levels can trigger cell death, we assessed cell viability by MTT assay. Our results demonstrated a significant decrease in viability only in HS astrocytes, with values of 58 ± 11 %, 70 ± 5 %, and 96 ± 0.1 % after 48, 72, and 120 h of treatment, respectively.

In contrast, in AD astrocytes, we observed a reduction in viability of

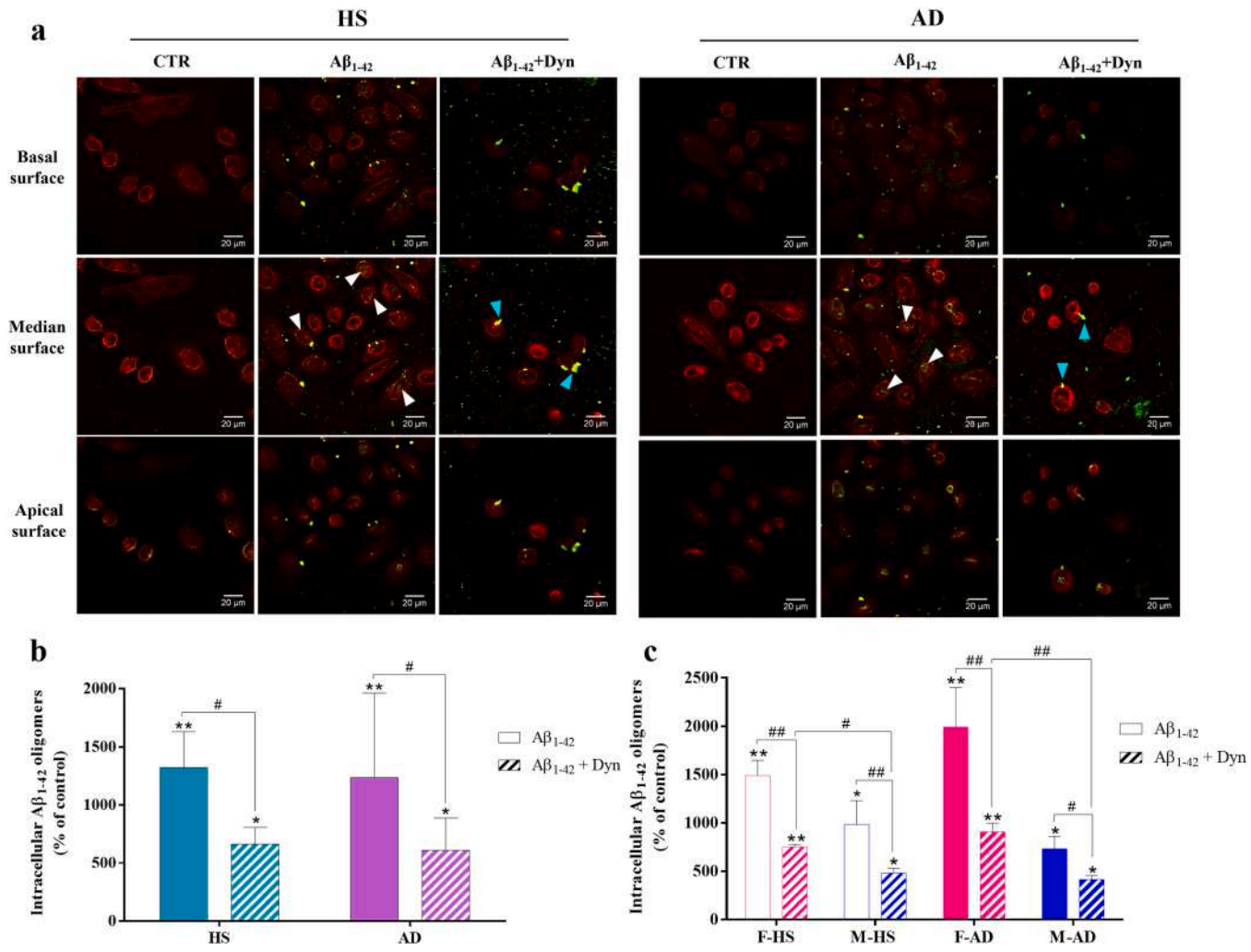

Fig. 2. Internalisation of $A\beta_{1-42}$ oligomers in human primary astrocytes treated with the endocytosis inhibitor dynasore. (a) Representative confocal scanning microscope images showing the basal, median and apical sections of control and treated astrocytes. Scale bars: 20 μm. (b) Semi-quantitative analysis of the $A\beta_{1-42}$-derived fluorescence expressed as the percentage of endogenous $A\beta_{1-42}$ fluorescence in astrocytes from healthy subjects and AD patients treated for 48 h with $A\beta_{1-42}$ oligomers in the presence or absence of dynasore 80 μM. (c) The graph illustrates the percentage of endogenous $A\beta_{1-42}$ fluorescence in treated astrocytes from healthy subjects and AD patients, stratified by sex. Data are expressed as the mean ± SD of two independent experiments. Statistical significance is indicated as follows: * $p < 0.05$ and ** $p < 0.001$ vs control (set to 100 %); # $p < 0.05$ and ## $p < 0.001$ for comparisons between treated cells. Abbreviations: CTR: control (untreated cells); HS: astrocytes from healthy subjects; AD: astrocytes from Alzheimer's patients; F-HS: astrocytes from female healthy subjects; M-HS: astrocytes from male healthy subjects; F-AD: astrocytes from female Alzheimer's patients; M-AD: astrocytes from male Alzheimer's patients; Dyn: dynasore 80 μM.

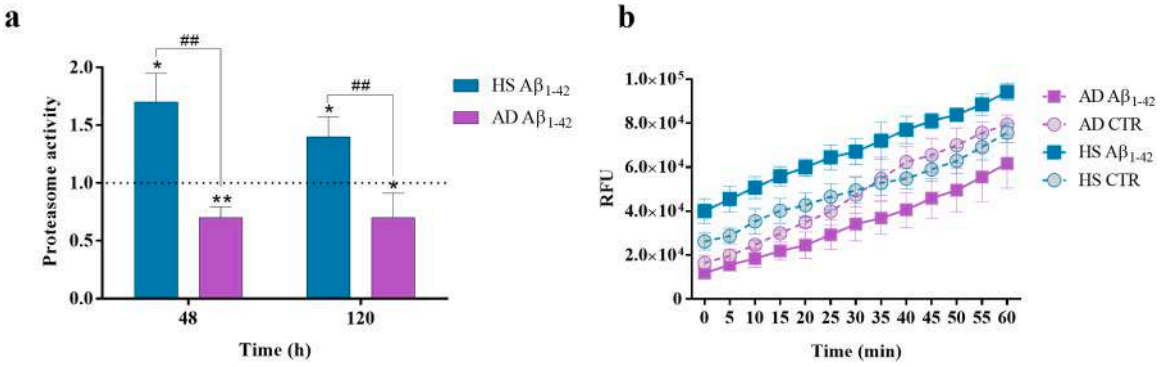

Fig. 3. Effects of $A\beta_{1-42}$ oligomers on proteasome activity. (a) The graph illustrates proteasome 20S activity after 48 and 120 h of treatment (relative to control, set to 1; dotted line) of astrocytes from 5 AD patients and 6 HS. (b) Relative fluorescent units of the proteasome activity assay were performed 48 h after the treatment. Statistical significance is indicated as follows: * $p < 0.05$ and ** $p < 0.001$ vs control (set to 1); # $p < 0.05$ and ## $p < 0.001$ for comparisons between treated cells; ns: not significant. Abbreviations: CTR: control (untreated cells); HS: astrocytes from healthy subjects; AD: astrocytes from Alzheimer's patients.

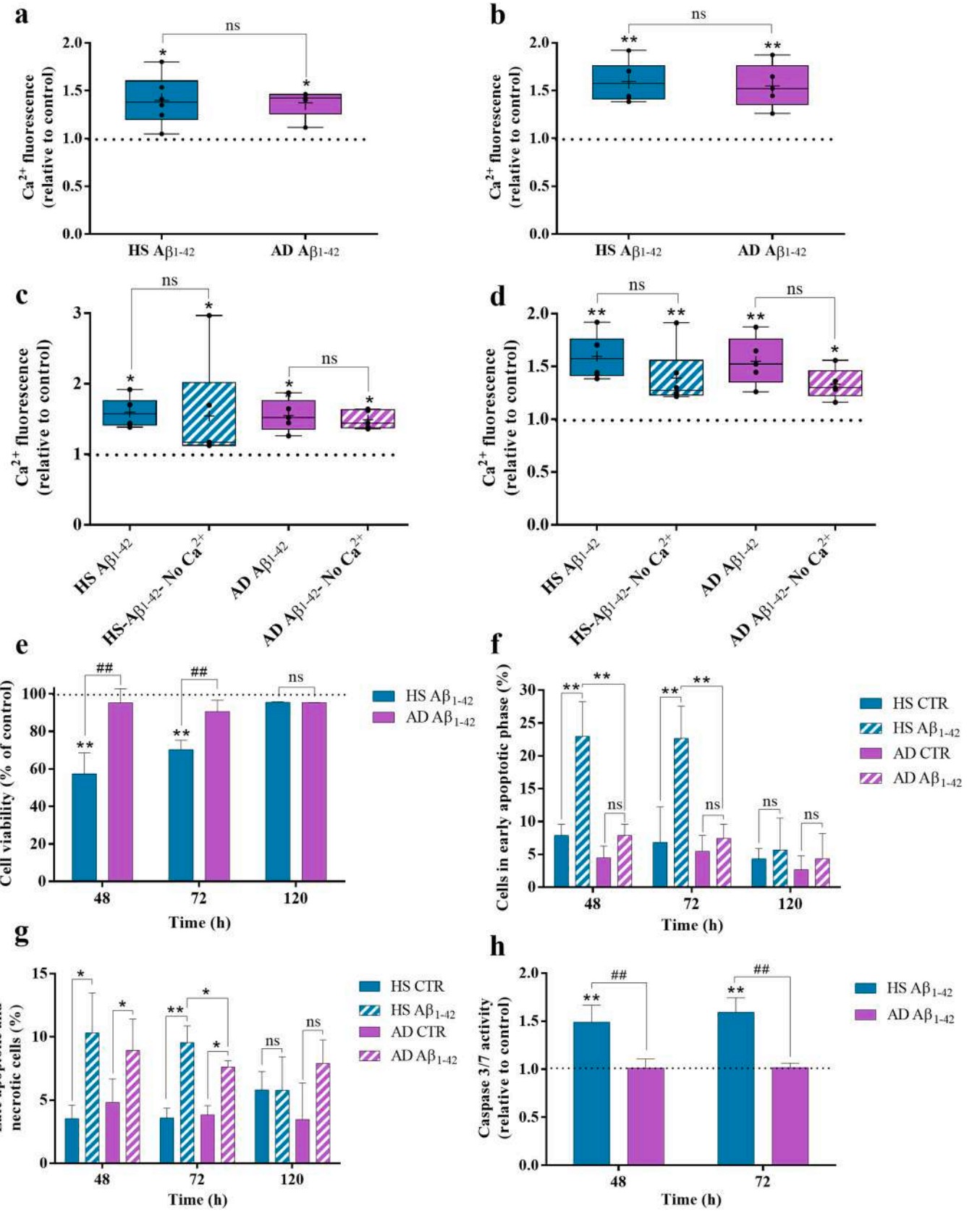

(caption on next page)

Fig. 4. Effect of $A\beta_{1-42}$ oligomers on calcium homeostasis, viability and apoptosis. Cytofluorimetric analysis of calcium levels in astrocytes from HS and AD patients after (a) 48 and (b) 72 h of treatment, assessed using Fluo-4 AM labelling. Graphs show calcium levels, expressed as median fluorescence intensity relative to control (set to 1; dotted line). Data are shown as box-and-whisker plots, with the box representing the interquartile range (IQR), the horizontal line indicating the median, and the whiskers extending to the minimum and maximum values. The mean is marked with a '+ ' symbol. Results were obtained from at least three independent experiments. (c, d) To determine whether the increase in calcium originated from intracellular release or extracellular influx, Fluo-4 AM was incubated in media with or without calcium. Graphs show calcium levels in astrocytes from HS and AD patients after (c) 48 and (d) 72 h of treatment, expressed as median fluorescence intensity relative to control (set to 1; dotted line). Data are shown as box-and-whisker plots, as reported in 4a and 4b. The mean is marked with a '+ ' symbol. Results were obtained from two independent experiments. (e) Graphs represent cell viability, performed by MTT assay, after 48, 72 and 120 h of treatment. Data are expressed relative to the control, set at 100 % (dotted line). (f-g) Graphs show the percentage of cells undergoing apoptosis/necrosis, assessed by Annexin V/7AAD cytofluorimetric assay after 48, 72, and 120 h of treatment. (f) Represents the percentage of cells in the early phase of apoptosis, while (g) shows the percentage of cells in late apoptosis/necrosis. (h) Caspase 3–7 activity was evaluated using Caspase-Glo® 3/7 kit after 48 and 72 h of treatment. Data are expressed relative to control activity (set to 1; dotted line). Data are presented as mean ± SD of three independent experiments. Statistical significance is indicated as follows: * $p < 0.05$ and ** $p < 0.001$ vs control; # $p < 0.05$ and ## $p < 0.001$ for comparisons between treated cells; ns: not significant. Abbreviations: CTR: control (untreated cells); HS: astrocytes from healthy subjects; AD: astrocytes from AD patients.

approximately 5 % at all time points, which was not statistically significant (Fig. 4e). To assess whether cell death occurred via the apoptotic process, we performed Annexin V/7AAD cytofluorimetric analysis. As shown in Fig. 4f, a significant increase in early apoptotic cells was observed in treated HS astrocytes at both 48 h (23 ± 5.3 %) and 72 h (22.7 ± 4.9 %) compared to untreated controls (7.8 ± 1.7 %

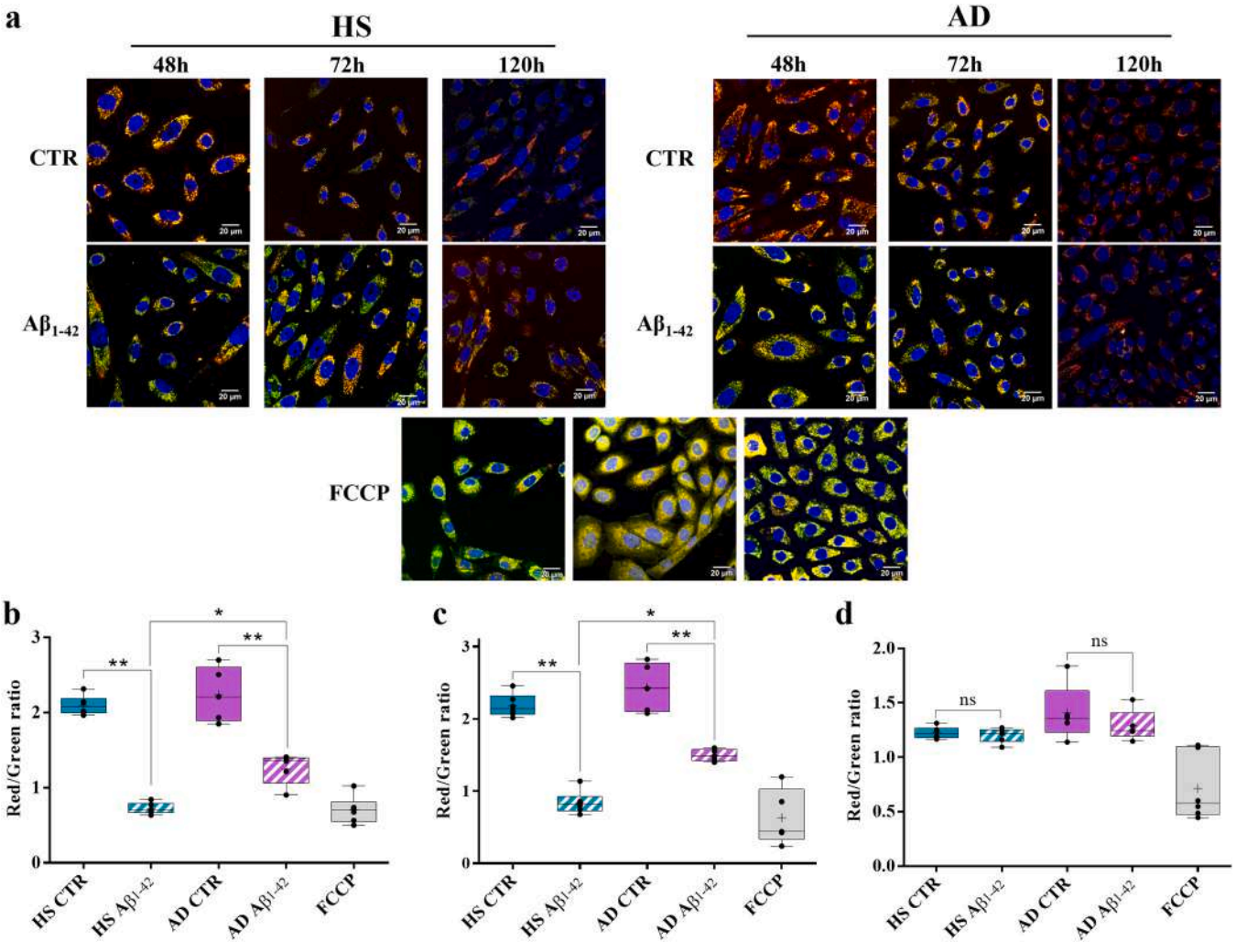

Fig. 5. Effect of $A\beta_{1-42}$ oligomers on mitochondrial membrane potential. (a) Representative confocal images of JC-1 fluorescence. Mitochondrial membrane potential was measured by JC-1, an indicator of mitochondrial function, in astrocytes from HS and AD patients treated with $A\beta_{1-42}$ oligomers for 48, 72, and 120 h. Red fluorescence represents the mitochondrial aggregate JC-1, and green fluorescence indicates the monomeric JC-1. A decrease in the red (~590 nm)/green (~529 nm) fluorescence intensity ratio indicates depolarisation of the mitochondrial membrane. We used an acute treatment with FCCP, a depolarising agent, as a positive control. Scale bars: 20 μm. Representative fields were selected to visualise JC-1 staining and do not reflect differences in cell number across conditions. (b-c-d) Graphs represent the ratio of aggregated and monomeric JC-1 (red/green), indicating changes in mitochondrial membrane potential after (b) 48, (c) 72, and (d) 120 h of treatment. Data are shown as box-and-whisker plots, with the box representing IQR, the horizontal line indicating the median, and the whiskers extending to the minimum and maximum values. The mean is marked with a '+ ' symbol. Each data point represents astrocytes derived from an individual patient (6 HS and 5 AD). Statistical significance is indicated as follows: * $p < 0.05$ and ** $p < 0.001$ vs control; # $p < 0.05$ and ## $p < 0.001$ for comparisons between treated cells; ns: not significant. Abbreviations: CTR: control (untreated cells); HS: astrocytes from healthy subjects; AD: astrocytes from AD patients.

and 6.8 ± 5.4 %, respectively). Notably, the percentage of early apoptotic cells in treated HS astrocytes was significantly higher than in treated AD astrocytes, which did not show any significant change compared to their respective controls at either time point. This suggests a resistance to the induction of early apoptosis in AD astrocytes. At 120 h, neither HS nor AD treated astrocytes displayed significant differences in early apoptosis compared to untreated controls.

Fig. 4g illustrates the results for late apoptosis/necrosis. In treated HS astrocytes, the percentage of late apoptotic/necrotic cells significantly increased at 48 h (10.3 ± 3.1 %) and 72 h (9.5 ± 1.3 %) compared to controls (3.5 ± 1.0 % and 3.6 ± 0.8 %, respectively). Treated AD astrocytes showed only a slight but significant increase in late apoptotic/necrotic cells at both 48 h (8.9 ± 2.5 % vs. 4.8 ± 1.9 %) and 72 h (7.6 ± 0.5 % vs. 3.8 ± 0.7 %) when compared to untreated AD cells, although values remained lower than those observed in treated HS astrocytes. At 120 h, the levels of late apoptotic/necrotic cells in both HS and AD treated astrocytes returned to baseline, becoming comparable to untreated controls. These findings were further corroborated by caspase-3/7 activity assays, which revealed a significant increase in caspase activation in treated HS astrocytes compared to both their controls (1.5-fold and 1.6-fold at 48 and 72 h, respectively) and treated AD astrocytes. In contrast, caspase-3/7 activation remained unchanged in treated AD astrocytes (1.01 and 1.02-fold at 48 and 72 h, respectively), indicating a negligible apoptotic response in these cells (Fig. 4h).

Considering the increased release of intracellular calcium and apoptosis rates in treated HS astrocytes, we assessed mitochondrial membrane potential using the JC-1 assay after 48, 72, and 120 h of treatment. Significant mitochondrial depolarisation was observed in astrocytes from both HS and AD at 48 and 72 h (Fig. 5a-d). However, the depolarisation was significantly more pronounced in HS astrocytes compared to AD astrocytes. Conversely, no changes were noted at 120 h.

3.3. $A\beta_{1-42}$ oligomers induce cellular senescence in AD astrocytes

Considering the absence of apoptosis in treated AD astrocytes and the observed alterations in calcium homeostasis, which influence cellular fate, we investigated whether $A\beta_{1-42}$ oligomers could trigger cellular senescence. We evaluated multiple senescence markers following 120 h of treatment with $A\beta_{1-42}$ oligomers to assess senescence induction. As illustrated in Fig. 6a-b, only AD astrocytes exhibited a significantly higher percentage of SA-β-Gal positive cells (24 ± 6 %) compared to the control (9 ± 2 %). In contrast, treated HS astrocytes did not show a significant presence of SA-β-Gal positive cells compared to the control (7 ± 3 % *vs* 4 ± 2 %). Consequently, we observed a significant increase in SA-β-Gal positive cells in treated AD compared to treated HS. Notably, sex-stratified analysis (Fig. 6c) revealed a significantly higher percentage of SA-β-Gal positive cells in F-AD (30 ± 2 %) compared to M-AD astrocytes (19 ± 2 %), suggesting a potential sex-dependent susceptibility to senescence induction. To further characterise the senescent phenotype, we analysed the expression of $p14^{ARF}$ by western blot (Fig. 6d; Supplementary Figure 2). The results showed a significant upregulation of $p14^{ARF}$ in treated AD astrocytes compared to control (1.6 ± 0.24) and treated HS astrocytes (1.02 ± 0.15), in which $p14^{ARF}$ level remained unchanged (Fig. 6e). In particular, the expression of $p14^{ARF}$ was higher in F-AD than in M-AD astrocytes (Fig. 6f). In parallel, we assessed the presence of γH2AX nuclear foci, a marker of DNA damage, and macroH2A.1 foci, which form the senescence-associated heterochromatin foci (SAHF), using confocal microscopy (Fig. 6g-n). Treated AD astrocytes exhibited a significant increase in the percentage of cells positive for both γH2AX and macroH2A.1 foci (27 ± 4 % and 19 ± 4 %, respectively) compared to control (13 %±2 and 9 ± 4 %, respectively) and treated HS astrocytes (15 ± 2 % and 9 ± 3 %, respectively) (Fig. 6h, m). Consistent with the previous findings, a sex difference was observed exclusively in AD astrocytes, with F-AD exhibiting a significantly higher number of γH2AX and macroH2A.1 foci positive cells compared to M-AD (Fig. 6i,n).

These findings seem to indicate that $A\beta_{1-42}$ oligomers exclusively induce cellular senescence in astrocytes from AD patients. To further support these findings, multiple linear regression analyses were performed to evaluate the contributions of donor age and pathological condition on senescence markers. The results, summarised in Supplementary Figure 3, indicate that senescence-associated parameters were more associated with the pathological condition than with donor age, which showed no significant effect. However, the small sample size can limit the strength and generalizability of the conclusions.

3.4. SASP factor expression, neuroinflammatory profile, and reactive astrogliosis in astrocytes following $A\beta_{1-42}$ oligomers treatment

Afterwards, we analysed some of the principal SASP factors and important brain molecules involved in neuroinflammation using a Quantibody array. The heatmap representation of the detected molecules in astrocytes from HS and AD revealed significant differences in expression patterns (Fig. 7). In AD astrocytes, we observed a significant upregulation of GDNF, CTNF, β-NGF, IL-10, IFN-γ, Eotaxin, Eotaxin-2, MCP-1, TNF-α, IL-1α, and IL-8, while BDNF expression was significantly decreased. In contrast, in HS astrocytes, we detected a significant increase in GDNF, CTNF, IL-10, Eotaxin, MCP-1, TNF-α, IL-1α, IL-8, TIMP-1, TGF-β, and MMP-3, whereas Eotaxin-2 was significantly reduced. When comparing HS and AD astrocytes, significant differences were identified in BDNF, TNF-α, Eotaxin-2, IL-10, and GDNF expression, highlighting distinct inflammatory and neurotrophic responses between these conditions (Fig. 7a). Additionally, sex-based differences were evident in some factor expressions. In AD astrocytes, GDNF and MCP-1 levels were significantly higher in females than in males, whereas GM-CSF, IL-10, MMP-3, and MMP-2 were significantly lower in females than in males. Similarly, in HS astrocytes, GDNF, IL-10, TGF-β, and MMP-3 were significantly elevated in females compared to males, while β-NGF and EGF levels were higher in males than in females (Fig. 7b).

To summarise these complex molecular profiles more effectively, we calculated cumulative $\log_2$ scores for pro-inflammatory, anti-inflammatory, and neurotrophic factors in $A\beta_{1-42}$-treated astrocytes (Table 2). Astrocytes from AD showed a slightly stronger pro-inflammatory response than HS and a modestly higher anti-inflammatory response. Interestingly, neurotrophic factors were better preserved in HS astrocytes, while their expression was markedly reduced in the AD group, suggesting a compromised neuroprotective capacity in the diseased condition. These cumulative scores reflect the distinct inflammatory and neurotrophic trajectories observed in the heatmap profiles.

Notably, since senescence was observed exclusively in AD astrocytes, the elevated expression of these neuroinflammatory factors in treated HS astrocytes was unexpected. We therefore investigated whether this increase could be linked to a chronic $A\beta_{1-42}$ activated state of astrocytes, which is often associated with morphological and functional changes, including increased proliferation. First, we performed cell counts at 48, 72, and 120 h of treatment (Fig. 8a). The graph and the table show that the number of treated HS astrocytes significantly decreased at 48 (27×10^3 *vs* 47×10^3 cells in untreated control) and 72 h (41×10^3 *vs* 65×10^3 cells in untreated control). These results are aligned with previous findings showing increased apoptosis and cell death (Fig. 4e-h). However, by 120 h, the number of treated HS astrocytes exceeded that of the control (15×10^4 *vs* 13×10^4), suggesting that the surviving cells recovered and underwent compensatory hyperproliferation. Notably, the number of HS astrocytes at 120 h was significantly higher than at 48 and 72 h ($p < 0.001$). The presence of hyperproliferative reactive astrocytes in HS was further supported by increased expression of GFAP and Vimentin (Fig. 8b) and by a significant positive correlation between GFAP fluorescence intensity and the number of Ki-67-positive cells, a proliferation marker. Notably, treated HS astrocytes exhibited the highest GFAP levels and a larger number of Ki-67-positive cells than control and AD astrocytes, as shown in the correlation analysis (Fig. 8c).

In contrast, treated AD astrocytes exhibited a significant reduction in

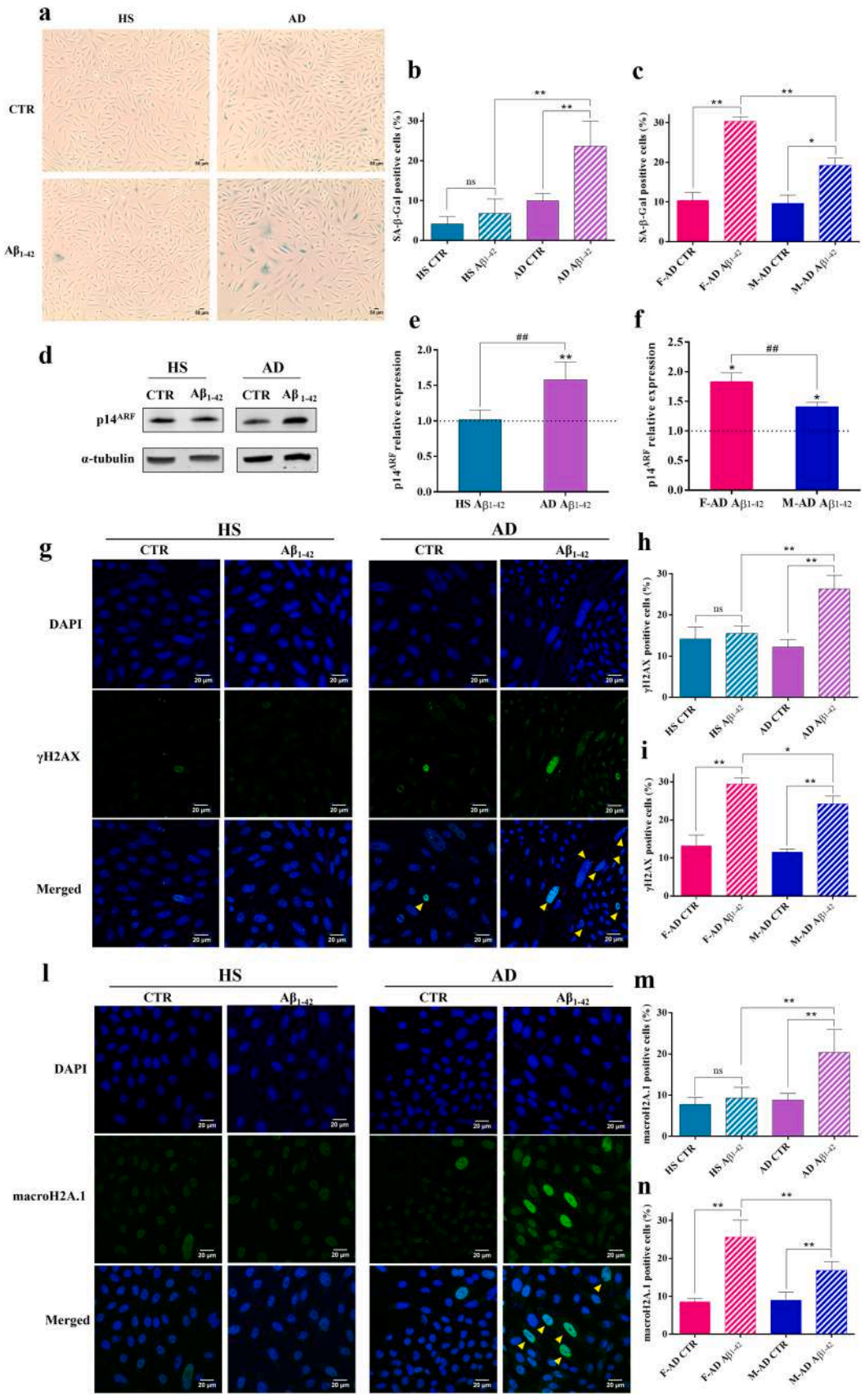

(caption on next page)

Fig. 6. Evaluation of senescence markers in astrocytes following $A\beta_{1-42}$ oligomers treatment. (a) Representative images of SA-β-Gal activity performed 120 h of $A\beta_{1-42}$-treatment. Scale bars: 50 μm. (b) The percentage of SA-β-Gal positive cells (blue ones) with respect to the total number of cells/well. (c) Percentage of SA-β-Gal positive cells after $A\beta_{1-42}$ treatment in astrocytes from AD stratified by sex. (d) Immunoblot representative images of $p14^{ARF}$ after 120 h of treatment. (e) The graph shows the quantification of $p14^{ARF}$ expression in astrocytes from HS and AD. Panel (f) presents a separate analysis of AD astrocytes stratified by sex. Protein band intensity was normalised to α-tubulin and expressed in relation to control (dotted line). (g) Representative confocal microscopy images of indirect immunofluorescence of γH2A1 foci (green), after 120 h of $A\beta_{1-42}$ treatment. DNA was counterstained with DAPI (blue). Scale bars: 20 μm. (h) Graph shows the percentage of γH2A1 foci positive cells in astrocytes from HS and AD patients. (i) Percentage of γH2A1 foci positive cells after $A\beta_{1-42}$ treatment in astrocytes from AD stratified by sex. (l) Representative confocal microscopy images of indirect immunofluorescence of macroH2A.1 foci (green) after 120 h of $A\beta_{1-42}$ treatment. DNA was counterstained with DAPI (blue). Scale bars: 20 μm. (m) Graph shows the percentage of macroH2A.1 foci positive cells in astrocytes from HS and AD patients. (n) Percentage of macroH2A.1 foci positive cells after $A\beta_{1-42}$ treatment in astrocytes from AD stratified by sex. Data are represented as the mean ± SD of three independent experiments. Statistical significance is indicated as follows: * $p < 0.05$ and ** $p < 0.001$ vs control; # $p < 0.05$ and ## $p < 0.001$ for comparisons between treated cells; ns: not significant. Abbreviations: CTR: control (untreated cells); HS: astrocytes from healthy subjects; AD: astrocytes from AD patients; F-AD: astrocytes from female AD patients; M-AD: astrocytes from male AD patients.

cell number at both 72 and 120 h (51×10^3 *vs* 65×10^3 cells in untreated control and 11×10^4 *vs* 14×10^4 cells in untreated control, respectively). Moreover, the number of AD astrocytes at 72 and 120 h was significantly lower than at 48 h ($p < 0.001$) (Fig. 8a). Upon treatment, a subset of AD astrocytes probably entered a state of cellular senescence, thereby losing their proliferative capacity. Multiple linear regression analyses, while acknowledging the limitations mentioned above, further supported these observations by showing that pathological condition was a consistent and significant predictor of increased Vimentin expression, Ki-67 positivity, and the overall astrogliosis index. In contrast donor age did not exert a significant effect (see Supplementary Figure 4). Interestingly, GFAP expression alone showed no significant association with pathological condition or age, suggesting it may not fully reflect the complex and stage-dependent nature of reactive astrogliosis, which likely requires multiple markers for comprehensive assessment.

3.5. *Effects of conditioned medium from treated HS and AD astrocytes on differentiated neuroblastoma cells (SH-SY5Y)*

After verifying the effects of $A\beta_{1-42}$ oligomers on astrocytes from HS and AD donors, we investigated whether their CM could influence the viability of SH-SY5Y differentiated into neuron-like cells. Astrocytes were treated with $A\beta_{1-42}$ oligomers for 120 h, after which the culture medium was replaced, and CM was collected after an additional 24 h (Fig. 9a). Differentiated SH-SY5Y cells, whose differentiation was confirmed by an increase in β3-tubulin fluorescence observed via confocal microscopy (Fig. 9b), were exposed to the collected CM for 24 h, and cell viability was evaluated using the MTT assay. Our results demonstrated that CM from treated AD astrocytes significantly reduced SH-SY5Y viability (73 ± 8 %) compared to CM from untreated AD astrocytes (100 %), whereas CM from treated HS astrocytes did not induce any significant change in cell viability (Fig. 9c). To further investigate the impact of CM on differentiated SH-SY5Y survival, we performed flow cytometry analysis to assess apoptotic and necrotic death after 24 h of exposure to CM. As shown in Fig. 9d, CM from treated HS astrocytes did not increase apoptosis compared to CM from control HS astrocytes. In contrast, CM from treated AD astrocytes significantly increased the percentage of apoptotic cells compared to both CM from untreated AD astrocytes and CM from treated HS astrocytes. This finding indicates a different effect of HS and AD astrocytes on neuronal cells.

4. Discussion

Aging is a progressive process that leads to the accumulation of molecular and cellular damage and represents the leading risk factor for ARDs, including AD, the most common form of dementia, which has a higher prevalence in women (Franceschi et al., 2018; Ostan et al., 2008; Qiu et al., 2009). The amyloid hypothesis proposes that Aβ aggregation, particularly in soluble oligomers, drives neurotoxicity and neuronal death (Chiti and Dobson, 2017; Lane et al., 2018; Querol-Vilaseca et al., 2019). Astrocytes, which play an essential role in brain homeostasis, undergo morphological and functional changes in AD, contributing to disease onset and progression (Acosta et al., 2017; Sofroniew and Vinters, 2010).

To our knowledge, this is one of the few studies investigating the effect of $A\beta_{1-42}$ oligomers on human primary astrocytes from HS and AD patients, aiming to understand whether they exhibit differential responses to $A\beta_{1-42}$-induced stress. While we acknowledge that the age range differs between HS and AD donors, we performed statistical analyses to evaluate the potential confounding role of age. These analyses suggest that the main differences observed between HS and AD astrocytes are more strongly associated with the pathological condition than with donor age, which did not appear to exert a significant effect.

We demonstrated that both HS and AD astrocytes can internalise $A\beta_{1-42}$ oligomers, with a higher uptake observed in F-AD astrocytes. Consistently, astrocytes have been shown to internalise $A\beta_{1-42}$ aggregates, including oligomers, in different models (Domínguez-Prieto et al., 2018; Griffin et al., 2020; Montoliu-Gaya et al., 2017; Mun et al., 2024; Yslas et al., 2024). Notably, a previous study using adult astrocytes from AD and non-demented patients reported a preferential internalisation of Aβ oligomers over fibrils, with no significant difference between the two groups (Nielsen et al., 2010, 2009). However, the organelles and molecular pathways involved in the internalisation and subsequent degradation of Aβ oligomers remain largely unclear. In our study, we employed dynasore, a potent GTPase inhibitor that rapidly inhibits dynamin activity, which prevents clathrin-dependent endocytosis, to investigate the internalisation pathway further. Dynasore treatment significantly reduces $A\beta_{1-42}$ oligomer uptake in both astrocytes from HS and AD patients. Accordingly, while the uptake of Aβ oligomers by astrocytes is primarily believed to involve phagocytosis (Zhang et al., 2014), as seen in microglia (Familian et al., 2007), different studies have shown that oligomers can also be internalised via endocytosis, as indicated by the temperature-dependent nature of the process (Domínguez-Prieto et al., 2018; Nielsen et al., 2009). Furthermore, Domínguez-Prieto et al. demonstrated that the involved endocytic pathways exclude caveolae-mediated endocytosis, whereas the formation of clathrin-coated vesicles was essential for oligomer internalisation in rat primary astrocytes (Domínguez-Prieto et al., 2018). In our experiments, dynasore treatment did not completely abolish oligomer internalisation, suggesting the involvement of alternative pathways, such as clathrin- and dynamin-independent endocytosis (Jiang and Chen, 2009). Moreover, although dynasore reduced $A\beta_{1-42}$ oligomer uptake in both male and female astrocytes, its apparent lower efficacy in females likely reflects their intrinsically higher baseline uptake levels rather than a diminished response to the drug. Even after dynasore treatment, female astrocytes retained more internalised oligomers, suggesting that the relative reduction with endocytosis inhibition was comparable across sexes, but the absolute levels of internal oligomers remained higher due to sex-specific differences in uptake capacity. Although we observed sex-related differences, these findings should be interpreted with caution due to the small sample size and the exploratory nature of the analysis. Sex-based differences are reported only when statistically significant and should be considered descriptive insight rather than conclusive. Future research with larger, sex-balanced

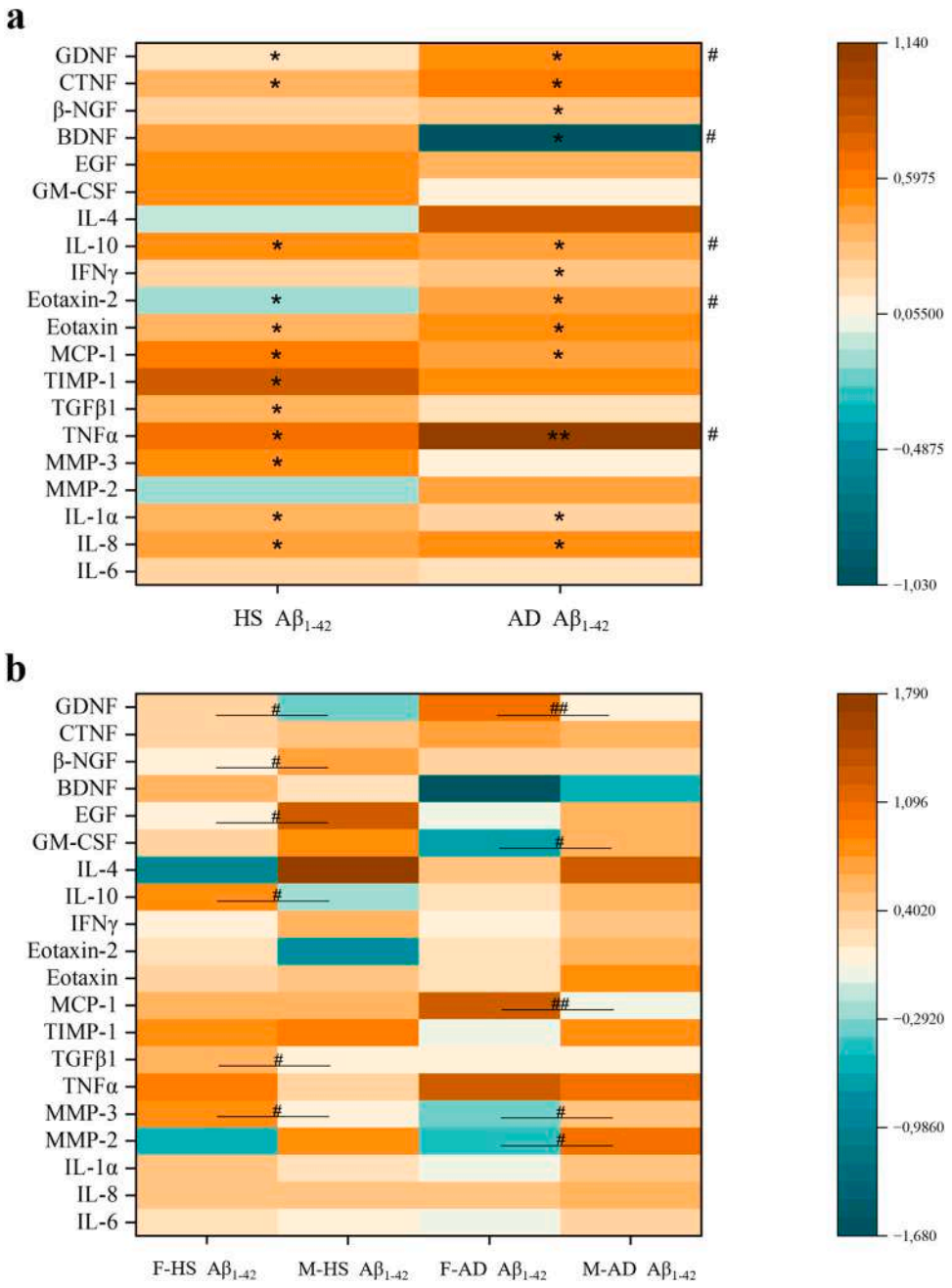

Fig. 7. SASP and neuroinflammatory factors production following $A\beta_{1-42}$ oligomers treatment. The production of SASP factors and neuroinflammatory molecules was assessed using a Quantibody array. (a) The heatmap shows the effect of 120 h of $A\beta_{1-42}$ treatment on the expression of secreted factors in astrocytes from 5 AD patients and 6 HS. (b) The heatmap depicts the same data, stratified by sex. Data are presented as the $\log_2$ fold change relative to the untreated control of astrocytes from 5 AD patients and 6 HS. Orange indicates upregulated expression, while blue represents downregulated expression relative to the untreated control. Statistical significance is shown as follows: * $p < 0.05$ and ** $p < 0.001$ vs control; # $p < 0.05$ and ## $p < 0.001$ for comparisons between treated cells. Abbreviations: HS: astrocytes from healthy subjects; AD: astrocytes from AD patients; F-HS: astrocytes from female healthy subjects; M-HS: astrocytes from male healthy subjects; F-AD: astrocytes from female AD patients; M-AD: astrocytes from male AD patients.

cohorts will be necessary to assess their biological relevance.

Despite their capacity to internalise Aβ oligomers, astrocytes may find it challenging to degrade them efficiently, accumulating intracellular aggregates (Rostami et al., 2021; Söllvander et al., 2018, 2016). Given the central role of the proteasome in protein degradation (Ben-Nissan and Sharon, 2014; Pickering and Davies, 2012), we examined its activity as a potential mechanism contributing to $A\beta_{1-42}$ clearance. Our data revealed a significant increase in proteasome activity in HS astrocytes, whereas in AD astrocytes, it was significantly impaired. These findings underscore a striking difference in response to $A\beta_{1-42}$ treatment, suggesting a compromised proteasomal function in the AD astrocytes. These results align with previous evidence showing proteasome dysfunction in the AD brain (Keller et al., 2000). Tseng et al. demonstrated that Aβ oligomers, but not monomers, inhibit proteasome activity *in vitro* and *in vivo* in a mouse model, leading to Aβ and tau accumulation (Tseng et al., 2008). Additionally, aggregated Aβ has been identified as a competitive substrate for the β5 chymotrypsin-like activity of the human 20S proteasome, suggesting that Aβ-induced proteasomal impairment may result from competition between endogenous substrates and accumulating toxic Aβ oligomers within AD cells (Zhao

Table 2
Cumulative log2 scores of pro-inflammatory, anti-inflammatory, and neurotrophic factors in human astrocytes from HS and AD patients treated with $A\beta_{1-42}$ oligomers. Scores represent the sum of log2 fold changes relative to untreated controls for all molecules included in each functional category. Pro-inflammatory molecules: IL-6, IL-8, IL-1α, TNFα, IFNγ, GM-CSF, MCP-1, Eotaxin, Eotaxin-2, MMP-2, and MMP-3; Anti-inflammatory molecules: IL-10, IL-4, and TGFβ1; Neurotrophic factors: BDNF, GDNF, β-NGF, CNTF, and EGF.

Category	HS $A\beta_{1-42}$ Score	AD $A\beta_{1-42}$ Score
Pro-inflammatory molecules	3.8	4.5
Anti-inflammatory molecules	0.8	1.4
Neurotrophic factors	1.8	0.8

and Yang, 2010).

While these studies strongly support the notion of proteasome impairment in AD, no previous evidence has reported an increase in proteasome activity following Aβ oligomers exposure, particularly in healthy astrocytes. The observed enhancement of proteasome function in treated HS astrocytes may suggest a more efficient proteostatic response, potentially facilitated by stress-induced upregulation of proteasomal components to address $A\beta_{1-42}$-related proteotoxicity. Nevertheless, the increase in proteasome activity observed in healthy astrocytes did not correspond to a reduction in intracellular $A\beta_{1-42}$, which may suggest that additional degradation or clearance mechanisms are necessary to eliminate $A\beta_{1-42}$ efficiently. However, further studies are needed to elucidate the molecular mechanisms involved in this process.

We subsequently examined changes in functional parameters, including calcium homeostasis, as dysregulated calcium levels are fundamental to astrocytic responses and affect many cellular processes (Alberdi et al., 2013; Kelly et al., 2023; Shrivastava et al., 2013). Our work demonstrated that $A\beta_{1-42}$ oligomers treatment increased intracellular free calcium levels in both HS and AD astrocytes. Interestingly, this increase was primarily due to release from intracellular reservoirs. Accordingly, several studies have shown that Aβ oligomers, including $A\beta_{1-40}$ and $A\beta_{1-42}$, induce intracellular calcium elevation in astrocytes even at low concentrations (Narayan et al., 2014). This calcium dysregulation is believed to result from the mobilisation of intracellular calcium, particularly from the endoplasmic reticulum (ER), via IP3 receptor activation (Narayan et al., 2014; Demuro et al., 2005; Kuchibhotla et al., 2009; Oseki et al., 2014). However, our investigations did not find an ER stress response (data not shown). One of the cellular processes potentially triggered by calcium dyshomeostasis is cell death. Interestingly, our findings demonstrate that apoptosis was selectively induced in HS astrocytes, albeit both HS and AD astrocytes exhibited a comparable increase in intracellular calcium levels after the treatment. Although the percentage of astrocytes undergoing late apoptosis/necrosis remained relatively low in both HS and AD groups (<10 %), we observed a significantly higher proportion of early apoptotic cells in HS astrocytes. This suggests an active apoptotic response that may not have fully progressed within the time window analysed. Nevertheless, we acknowledge that further time-resolved experiments will be required to more precisely define the temporal dynamics of $A\beta_{1-42}$ induced apoptosis in astrocytes. This observation aligns with previous studies reporting that the accumulation of neurotoxic Aβ fragments leads to cytoplasmic calcium mobilisation, ultimately triggering programmed cell death in astrocytes from *in vivo* models (Hong et al., 2023; Narayan et al., 2014; Oseki et al., 2014). Strikingly, these studies emphasise the ability of Aβ oligomers to promote apoptosis predominantly in healthy cells, consistent with our findings. However, the underlying mechanism rendering HS astrocytes more susceptible to $A\beta_{1-42}$ oligomer-induced apoptosis remains unclear and warrants further investigation. One possible explanation is that AD astrocytes, having been chronically exposed to Aβ *in vivo*, may have developed adaptive mechanisms that modify their responses and increase their resistance to apoptosis. In this context, we observed a significant decrease in mitochondrial membrane potential in treated astrocytes after 48 and 72 h of exposure. Importantly, this depolarisation occurred concurrently with increased intracellular calcium levels and may be partly responsible for this. The effect was particularly pronounced in HS astrocytes, where depolarisation was significantly greater than in AD astrocytes. The more substantial depolarisation in HS astrocytes likely triggered harmful effects that led to apoptosis, whereas in AD astrocytes, the depolarisation was insufficient to induce cell death. However, we found that $A\beta_{1-42}$ oligomers induced senescence in a subset of treated AD astrocytes but did not affect those from HS. This partially confirms previous findings by Ungerleider et al., who reported $A\beta_{1-42}$ oligomers-induced senescence in primary human astrocytes. However, important differences in experimental design and donor characterisation distinguish the two studies (Ungerleider et al., 2022). Notably, Ungerleider et al. employed human primary astrocytes without differentiating between healthy and diseased conditions, whereas our study used astrocytes from both cognitively healthy donors and AD patients, allowing for the identification of disease-specific responses to Aβ.

Moreover, Ungerleider et al. assessed senescence after a relatively short exposure (24 h of treatment followed by 72 h in fresh medium), whereas in our experimental design, astrocytes were continuously exposed to $A\beta_{1-42}$ oligomers for 5 days. This chronic exposure may better mimic the persistent amyloid burden in the AD brain and revealed distinct phenotypic outcomes, namely astrogliosis in healthy astrocytes and senescence in AD astrocytes. Overall, our results confirm the ability of $A\beta_{1-42}$ oligomers to trigger astrocyte senescence, as previously observed by Ungerleider et al., but extend those findings by demonstrating that this response is modulated by both the pathological background and the duration of exposure. In line with these observations, Bhat et al. also reported that $A\beta_{1-42}$ oligomers can induce senescence, although in human fetal astrocytes and under different experimental conditions (Bhat et al., 2012). Taken together, these studies support the notion that $A\beta_{1-42}$ oligomers are potent inducers of astrocyte senescence, while our findings add novel insights into the disease-specific and exposure-dependent aspects in adult human astrocytes. Nevertheless, to assess whether the observed increase in senescence markers was influenced by age rather than pathology, we performed multiple linear regression analyses including age and disease condition as predictors. The results showed that only the pathological condition was significantly associated with the expression of SA-β-Gal, $p14^{ARF}$, and SAHF, whereas age did not show any significant effect. This was also confirmed by a composite senescence index based on z-scores. The presence of senescent astrocytes is well-documented in *postmortem* AD brains, supporting the hypothesis that they contribute to neurodegeneration via pro-inflammatory signalling and/or disruption of glutamate homeostasis (Bhat et al., 2012; Gaikwad et al., 2018; Han et al., 2020; Limbad et al., 2020; Turnquist et al., 2016; Tuzer and Torres, 2022). Notably, we found a higher prevalence of senescent astrocytes in F-AD than in M-AD, as confirmed by multiple senescence markers studied. This aligns with evidence of sex differences in astrocyte morphology, gene expression, and function (Amateur and McCarthy, 2002; Arias et al., 2009; Beyer et al., 1990; Chowen et al., 1995) and suggests that female astrocytes may have distinct responses to pathological insults (Astiz et al., 2014; Chistyakov et al., 2018; Liu et al., 2007; Loram et al., 2012; Santos-Galindo et al., 2011). While most studies on sex differences rely on animal models, our findings provide novel insights using primary human astrocytes. Indeed, although constrained by a small sample size, our results suggest that sex-related differences in astrocyte senescence may contribute to the differential risk and progression of AD in men and women. These preliminary observations underscore the critical importance of recognising sex as a biological variable in future research aimed at elucidating the cellular mechanisms in AD pathology.

We then analysed SASP factors involved in neuroinflammation, including cytokines, metalloproteases and neurotrophic factors. Surprisingly, despite senescence being exclusive to AD astrocytes, SASP

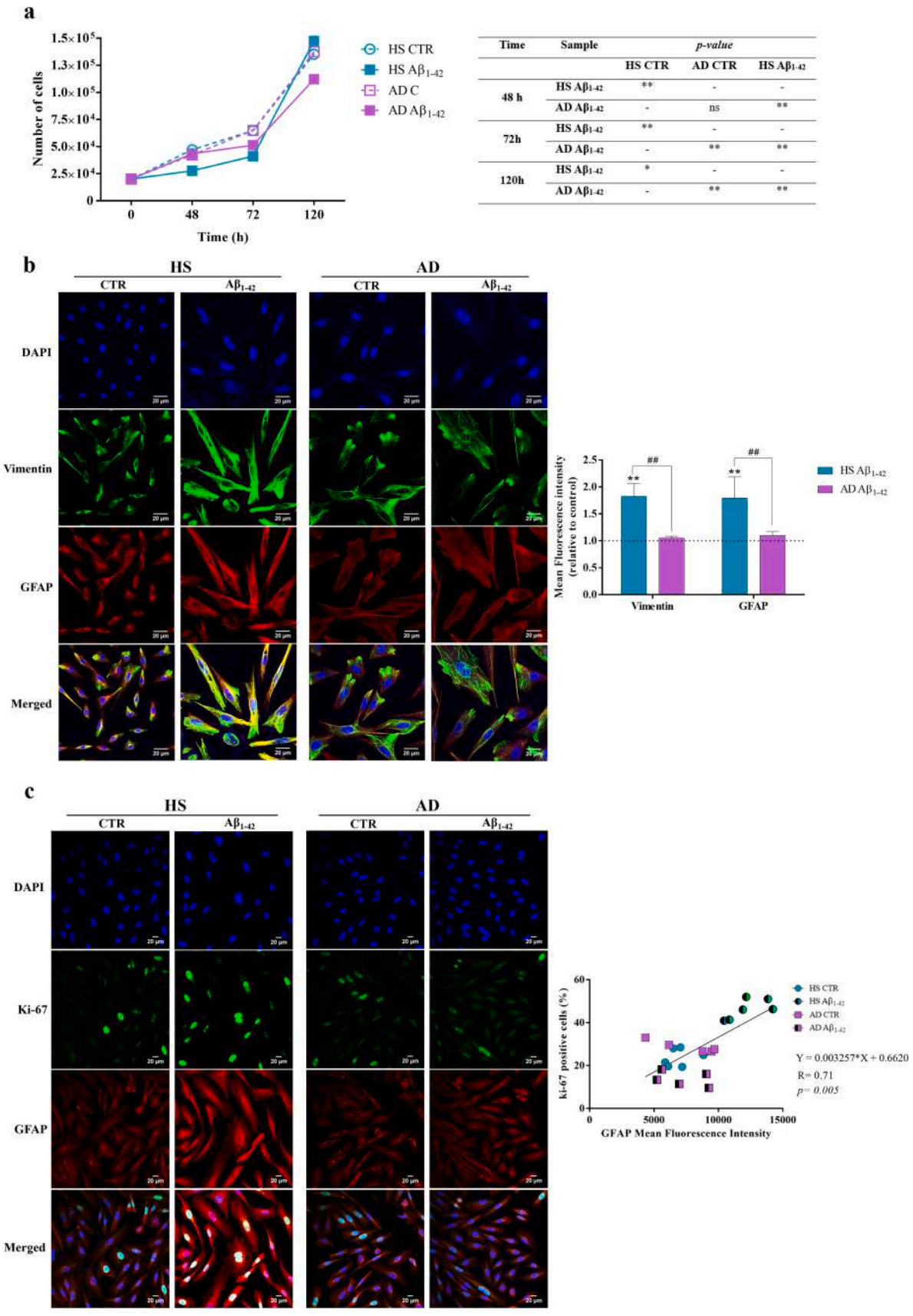

Time	Sample	p-value		
		HS CTR	AD CTR	HS Aβ1-42
48 h	HS Aβ1-42	**	-	-
	AD Aβ1-42	-	ns	**
72h	HS Aβ1-42	**	-	-
	AD Aβ1-42	-	**	**
120h	HS Aβ1-42	*	-	-
	AD Aβ1-42	-	**	**

(caption on next page)

Fig. 8. $A\beta_{1-42}$ oligomers induced astrogliosis in HS astrocytes. (a) The trypan blue exclusion assay was performed at three time points during treatment. The graph on the left shows cell proliferation in the different experimental groups over time, expressed as the number of viable cells per well. Data are presented as mean ± SD of three independent experiments. The table on the right summarises the statistical comparisons between groups, indicating the corresponding p-values (* $p < 0.05$ and ** $p < 0.001$). (b) Representative confocal microscopy images (left) of indirect immunofluorescence of Vimentin (green) and GFAP (red) after 120 h of $A\beta_{1-42}$ treatment. DNA was counterstained with DAPI (blue). Scale bars: 20 μm. On the right, the graph shows the mean fluorescence intensity of the two proteins expressed in relation to control (set as 1; dotted line). (c) Representative confocal microscopy images (left) of indirect immunofluorescence of Ki-67 (green) and GFAP (red) after 120 h of $A\beta_{1-42}$ oligomers treatment. DNA was counterstained with DAPI (blue). Scale bars: 20 μm. On the right, the graph shows the linear regression analysis of the mean fluorescence intensity of GFAP with the percentage of Ki-67 positive cells. Pearson correlation coefficient (R) and p-value are shown. Data are represented as the mean ± SD of three independent experiments. Statistical significance is indicated as follows: * $p < 0.05$ and ** $p < 0.001$ vs control; # $p < 0.05$ and ## $p < 0.001$ for comparisons between treated cells. Abbreviations: CTR: control (untreated cells); HS: astrocytes from healthy subjects; AD: astrocytes from Alzheimer's patients.

expression did not differ drastically between AD and HS. The most significant differences were observed in BDNF, a crucial neurotrophin involved in neuron survival, which was significantly increased in HS astrocytes and decreased in AD. Moreover, Eotaxin-2, a member of the Eotaxin family—known to be elevated in the plasma of AD patients and potentially involved in neurodegeneration (Huber et al., 2018)—was significantly reduced in HS but increased in AD. Additionally, TNF-α was upregulated in both HS and AD astrocytes, with a more pronounced increase in AD. These changes in individual molecules are also reflected in the cumulative $\log_2$ scores calculated for pro-inflammatory, anti-inflammatory, and neurotrophic factors. Notably, astrocytes from AD patients exhibited a slightly higher pro-inflammatory score than those from HS, indicating a more sustained or intensified inflammatory state. Interestingly, the anti-inflammatory score was also modestly elevated in AD, which may represent a compensatory but insufficient regulatory mechanism to reduce inflammation. In contrast, neurotrophic factor scores were markedly higher in HS astrocytes, suggesting that healthy cells maintain better neuroprotective signalling. These data suggest that both HS and AD astrocytes mount an inflammatory response after 120 h of $A\beta_{1-42}$ treatment. However, the balance between inflammatory and neurotrophic pathways differs substantially. AD astrocytes seem to experience a more persistent pro-inflammatory milieu coupled with impaired neurotrophic support. This situation may contribute to the neurodegenerative environment characteristic of AD. The imbalance between inflammation and neuroprotection could increase neuronal vulnerability and accelerate disease progression. Moreover, it is important to note that astrocytes, also following Aβ oligomers treatment, can also transition into a reactive state, which can be pro-inflammatory and detrimental to neurons (Liddelow and Barres, 2017; Mun et al., 2024; Ortiz-sanz et al., 2022; Osborn et al., 2016; Wyssenbach et al., 2016). It is well known that reactive and senescent astrocytes share common inflammatory features (López-Teros et al., 2024; Simmnacher et al., 2020). Our data suggest that HS astrocytes surviving $A\beta_{1-42}$-induced toxicity undergo hyperproliferation and adopt a reactive phenotype, as indicated by increased GFAP and Vimentin expression and by the release of pro-inflammatory factors. Pearson regression analysis supports this finding, showing a positive correlation between Ki-67 and GFAP in HS astrocytes, which confirms that proliferating cells exhibit reactive characteristics. In contrast, AD astrocytes fail to mount a reactive response but undergo senescence, possibly due to chronic Aβ exposure *in vivo*, leading to a higher damage threshold or impaired reactivity *in vitro*. Consistently, multiple linear regression analyses confirmed that the pathological condition, rather than donor age, was the main factor influencing the divergent astrocytic responses observed. Although these analyses were performed on a relatively small sample size ($n = 11$), which limits statistical power and generalizability, the consistent association of the pathological condition with both senescence and astrogliosis markers—independent of age—supports the presence of a disease-specific cellular phenotype. These results should therefore be considered preliminary and interpreted with appropriate caution.

Finally, we found that CM from senescent AD astrocytes effectively induced apoptosis in neuroblastoma cells differentiated to a neuron-like phenotype. In contrast, CM from HS astrocytes did not exhibit this effect. These findings indicate that CM from AD astrocytes may contain toxic, undetected molecules that contribute to neuronal cell death, reinforcing the notion that cellular changes in senescent AD astrocytes can release harmful factors impacting surrounding neural cells. Our observations support previous findings that senescent astrocytes drive neuroinflammation and neuronal death (Bhat et al., 2012; Bitto et al., 2010; Guerrero et al., 2021; Kawano et al., 2017; Limbad et al., 2020; Pertusa et al., 2007), with SASP factors contributing to neurodegeneration (Chinta et al., 2015; Han et al., 2024; Maciel-Barón et al., 2018; Zhang et al., 2022). Although the percentage of senescent cells induced by $A\beta_{1-42}$ in our model was relatively modest—particularly when compared to classical stress-induced premature senescence—the cells nonetheless exhibited a functionally relevant phenotype. Notably, this modest increase in SA-β-Gal positivity and other senescence markers was sufficient to trigger a pronounced neurotoxic response in recipient SH-SY5Y cells. Together, these findings suggest that even a limited number of senescent astrocytes may exert significant detrimental effects in the AD context, not only through direct toxicity but also via paracrine signalling and SASP-mediated propagation. Thus, the modest senescence observed *in vitro* may still reflect a biologically relevant phenomenon, with potential implications for neuroinflammation and tissue homeostasis in AD. Further studies in co-culture or *in vivo* models will be essential to assess these indirect effects fully. Interestingly, despite comparable SASP levels in AD and HS astrocytes, only AD CM induced neurotoxicity, suggesting that unidentified factors beyond the studied SASP components may drive neuronal damage. This highlights the need for further investigations into the toxic secretome of senescent AD astrocytes. Such research could improve our understanding of the disease progression and help identify potential therapeutic intervention targets.

In conclusion, our study demonstrates that $A\beta_{1-42}$ oligomers elicit distinct responses in human HS and AD astrocytes, including differential alterations in proteasomal activity, despite similar levels of oligomer internalisation. Importantly, while intracellular calcium increase was comparable between the two groups, a subset of HS astrocytes underwent apoptosis. In contrast, the surviving cells developed a reactive, hyperproliferative state, producing neuroinflammatory factors, likely as a compensatory mechanism to counteract damage and the loss of astrocytes. Conversely, AD astrocytes, having likely been previously exposed to oligomers *in vivo*, exhibited resistance to apoptosis but lost the ability to become reactive, thereby failing to compensate for damage. Instead, these cells entered a senescent state, producing neuroinflammatory factors at levels comparable to HS reactive astrocytes. However, their conditioned medium was uniquely capable of inducing differentiated neuroblastoma cell death. Therefore, although our study has been conducted in a limited number of cases due to the reduced availability of human astrocytes, our findings highlight the importance of further investigating these models to gain deeper insights into the differences between healthy and AD-affected astrocytes. This approach may provide critical insights into disease-specific mechanisms and inform the development of novel therapeutic strategies.

CRediT authorship contribution statement

Alessandra Bigi: Writing – review & editing, Methodology,

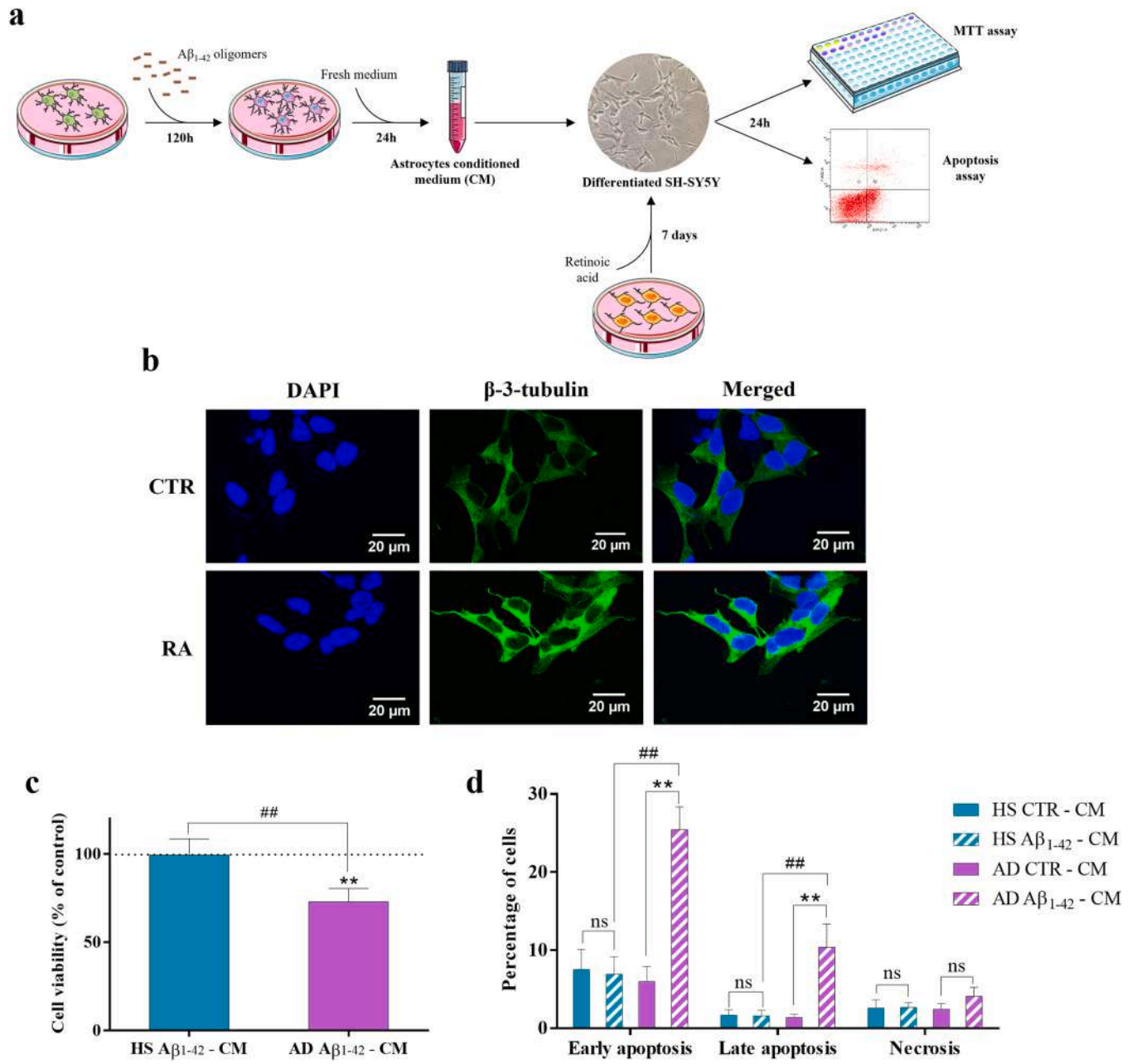

Fig. 9. Effects of CM from HS and AD treated astrocytes on differentiated SH-SY5Y neuron-like cells. (a) Experimental scheme. After 120 h of treatment with $A\beta_{1-42}$ oligomers, culture medium was replaced with a fresh one for 24 h. Subsequently, CM was collected and used to treat differentiated SH-SY5Y neuron-like cells. Following 24 h of treatment, cell viability and apoptosis rate were verified. (b) Representative confocal microscopy images of β-3-tubulin immunofluorescence (green) in SH-SY5Y cells. Non-differentiated control cells and differentiated neuron-like cells for 7 days with RA (10 μM) and 1 % FBS are shown. DNA was counterstained with DAPI (blue). Scale bars: 20 μm. (c) Graphs represent cell viability, performed by MTT assay, after 24 h of treatment. Data are expressed relative to the control cells treated with CM from untreated astrocytes (set at 100 %; dotted line). (d) Graphs show the percentage of cells undergoing apoptosis/necrosis, assessed by Annexin V/7AAD cytofluorimetric assay after 24 h of treatment. Data are represented as the mean ± SD of three independent experiments. Statistical significance is indicated as follows: * $p < 0.05$ and ** $p < 0.001$ vs control; # $p < 0.05$ and ## $p < 0.001$ for comparisons between treated cells. Abbreviations: CTR: control (untreated cells); HS: astrocytes from healthy subjects; AD: astrocytes from AD patients; CM: conditioned medium; RA: retinoic acid.

Investigation. **Daniela Monti:** Writing – review & editing, Supervision, Resources, Project administration, Funding acquisition, Conceptualization. **Luisa Iommarini:** Writing – review & editing. **Manuela Sollazzo:** Writing – review & editing. **Cristina Cecchi:** Writing – review & editing, Funding acquisition, Conceptualization. **Elisa Bientinesi:** Writing – review & editing, Visualization, Validation, Investigation, Formal analysis, Conceptualization. **Gianmarco Bertoni:** Validation, Methodology. **Sara Ristori:** Writing – original draft, Methodology, Formal analysis, Conceptualization.

Fundings

This work was supported by internal funding from the University of Florence as well as co-funded by Next Generation EU, in the context of the National Recovery and Resilience Plan, Investment Partenariato Esteso PE8 -Project Age-IT: "Ageing Well in an Ageing Society". This resource was co-financed by the Next Generation EU [DM 1557 11.10.2022] to D.M. and project MNESYS (PE0000006) - A Multiscale integrated approach to the study of the nervous system in health and disease (D.R. 1553, 11.10.2022) to C.C. Manuela Sollazzo is supported

by the European Union – Next Generation EU through the Italian Ministry of University and Research under PNRR - M4C2- I1.3 Project PE_00000019 “HEAL ITALIA”. The views and opinions expressed are only those of the authors and do not necessarily reflect those of the European Union or the European Commission. Neither the European Union nor the European Commission can be held responsible for them.

Declaration of Competing Interest

The authors declare no competing interests.

Appendix A. Supporting information

Supplementary data associated with this article can be found in the online version at doi:10.1016/j.mad.2025.112116.

Data availability

Data will be made available on request.

References

Acosta, C., Anderson, H.D., Anderson, C.M., 2017. Astrocyte dysfunction in Alzheimer disease. J. Neurosci. Res. 95, 2430–2447. https://doi.org/10.1002/JNR.24075.

Alberdi, E., Wyssenbach, A., Alberdi, M., Sánchez-Gómez, M.V., Cavaliere, F., Rodríguez, J.J., Verkhratsky, A., Matute, C., 2013. Ca2+-dependent endoplasmic reticulum stress correlates with astrogliosis in oligomeric amyloid β-treated astrocytes and in a model of Alzheimer’s disease. Aging Cell 12, 292–302. https://doi.org/10.1111/ACEL.12054.

Alzheimer Association, 2020. 2020 Alzheimer’s disease facts and figures. Alzheimer’S. Dement 16, 391–460. https://doi.org/10.1002/alz.12068.

Amateur, S.K., McCarthy, M.M., 2002. Sexual differentiation of astrocyte morphology in the developing rat preoptic area. J. Neuroendocr. 14, 904–910. https://doi.org/10.1046/j.1365-2826.2002.00858.x.

Anderson, M.A., Ao, Y., Sofroniew, M.V., 2013. Heterogeneity of reactive astrocytes. Neurosci. Lett. 0, 23–29. https://doi.org/10.1016/J.NEULET.2013.12.030.

Arias, C., Zepeda, A., Hernández-Ortega, K., Leal-Galicia, P., Lojero, C., Camacho-Arroyo, I., 2009. Sex and estrous cycle-dependent differences in glial fibrillary acidic protein immunoreactivity in the adult rat hippocampus. Horm. Behav. 55, 257–263. https://doi.org/10.1016/j.yhbeh.2008.10.016.

Astiz, M., Acaz-Fonseca, E., Garcia-Segura, L.M., 2014. Sex differences and effects of estrogenic compounds on the expression of inflammatory molecules by astrocytes exposed to the insecticide dimethoate. Neurotox. Res. 25, 271–285. https://doi.org/10.1007/s12640-013-9417-0.

Barnes, L.L., Wilson, R.S., Bienias, J.L., Schneider, J.A., Evans, D.A., Bennett, D.A., 2005. Sex differences in the clinical manifestations of Alzheimer disease pathology. Arch. Gen. Psychiatry 62, 685–691. https://doi.org/10.1001/archpsyc.62.6.685.

Barragán Martínez, D., García Soldevilla, M.A., Parra Santiago, A., Tejeiro Martínez, J., 2019. Alzheimer’s disease. Med, 12, 4338–4346. https://doi.org/10.1016/j.med.2019.03.012.

Ben-Nissan, G., Sharon, M., 2014. Regulating the 20S proteasome Ubiquitin-Independent degradation pathway. Biomolecules 4, 862. https://doi.org/10.3390/BIOM4030862.

Beyer, C., Epp, B., Fassberg, J., Reisert, I., Pilgrim, C., 1990. Region- and sex-related differences in maturation of astrocytes in dissociated cell cultures of embryonic rat brain. Glia 3, 55–64. https://doi.org/10.1002/glia.440030108.

Bhat, R., Crowe, E.P., Bitto, A., Moh, M., Katsetos, C.D., Garcia, F.U., Johnson, F.B., Trojanowski, J.Q., Sell, C., Torres, C., 2012. Astrocyte senescence as a component of Alzheimer’s disease. PLoS One 7, e45069. https://doi.org/10.1371/journal.pone.0045069.

Bigi, A., Loffredo, G., Cascella, R., Cristina, C., 2020. Targeting pathological amyloid aggregates with Conformation-Sensitive antibodies. Curr. Alzheimer Res 17, 722–734.

Bigi, A., Lombardo, E., Cascella, R., Cecchi, C., 2023. The toxicity of protein aggregates: new insights into the mechanisms. Int J. Mol. Sci. 24, 7974. https://doi.org/10.3390/ijms24097974.

Bitto, A., Sell, C., Crowe, E., Lorenzini, A., Malaguti, M., Hrelia, S., Torres, C., 2010. Stress-induced senescence in human and rodent astrocytes. Exp. Cell Res. 316, 2961–2968. https://doi.org/10.1016/j.yexcr.2010.06.021.

Bussian, T.J., Aziz, A., Meyer, C.F., Swenson, B.L., van Deursen, J.M., Baker, D.J., 2018. Clearance of senescent glial cells prevents tau-dependent pathology and cognitive decline. Nature 562, 578–582. https://doi.org/10.1038/s41586-018-0543-y.

Cevenini, E., Monti, D., Franceschi, C., 2013. Inflamm-ageing. Curr. Opin. Clin. Nutr. Metab. Care 16, 14–20. https://doi.org/10.1097/MCO.0b013e32835ada13.

Chinta, S.J., Woods, G., Rane, A., Demaria, M., Campisi, J., Andersen, J.K., 2015. Cellular senescence and the aging brain. Exp. Gerontol. 68, 3–7. https://doi.org/10.1016/j.exger.2014.09.018.

Chistyakov, D.V., Azbukina, N.V., Astakhova, A.A., Goriainov, S.V., Chistyakov, V.V., Sergeeva, M.G., 2018. Sex-Mediated differences in LPS induced alterations of TNFα, IL-10 expression, and prostaglandin synthesis in primary astrocytes. Int. J. Mol. Sci. 19, 2793. https://doi.org/10.3390/IJMS19092793.

Chiti, F., Dobson, C.M., 2017. Protein misfolding, amyloid formation, and human disease: a summary of progress over the last decade. Annu. Rev. Biochem. 86, 27–68. https://doi.org/10.1146/ANNUREV-BIOCHEM-061516-045115/1.

Chowen, J.A., Busiguina, S., García-Segura, L.M., 1995. Sexual dimorphism and sex steroid modulation of glial fibrillary acidic protein messenger RNA and immunoreactivity levels in the rat hypothalamus. Neuroscience 69, 519–532. https://doi.org/10.1016/0306-4522(95)00250-M.

Cohen, J., Torres, C., 2019. Astrocyte senescence: evidence and significance. Aging Cell. https://doi.org/10.1111/acel.12937.

Cossarizza, A., Baccarini-Contri, M., Kalashnikova, G., Franceschi, C., 1993. A new method for the cytofluorimetric analysis of mitochondrial membrane potential using the J-aggregate forming lipophilic cation 5,5’,6,6’-tetrachloro-1,1’,3,3’-tetraethylbenzimidazolcarbocyanine iodide (JC-1). Biochem Biophys. Res Commun. 197, 40–45.

Csipo, T., Lipecz, A., Ashpole, N.M., Balasubramanian, P., Tarantini, S., 2020. Astrocyte senescence contributes to cognitive decline. GeroScience. https://doi.org/10.1007/s11357-019-00140-9.

Demuro, A., Mina, E., Kayed, R., Milton, S.C., Parker, I., Glabe, C.G., 2005. Calcium dysregulation and membrane disruption as a ubiquitous neurotoxic mechanism of soluble amyloid oligomers. J. Biol. Chem. 280, 17294–17300. https://doi.org/10.1074/jbc.M500997200.

Dimri, G.P., Lee, X., Basile, G., Acosta, M., Scott, G., Roskelley, C., Medrano, E.E., Linskens, M., Rubelj, I., Pereira-Smith, O., Al, E., 1995. A biomarker that identifies senescent human cells in culture and in aging skin in vivo. Proc. Natl. Acad. Sci. U. S. A. 92, 9363–9367.

Domínguez-Prieto, M., Velasco, A., Tabernero, A., Medina, J.M., 2018. Endocytosis and transcytosis of Amyloid-β peptides by astrocytes: a possible mechanism for Amyloid-β clearance in Alzheimer’s disease. J. Alzheimer’S. Dis. 65, 1109–1124. https://doi.org/10.3233/JAD-180332.

Escartin, C., Galea, E., Lakatos, A., O’Callaghan, J.P., Petzold, G.C., Serrano-Pozo, A., Steinhäuser, C., Volterra, A., Carmignoto, G., Agarwal, A., Allen, N.J., Araque, A., Barbeito, L., Barzilai, A., Bergles, D.E., Bonvento, G., Butt, A.M., Chen, W.T., Cohen-Salmon, M., Cunningham, C., Deneen, B., De Strooper, B., Díaz-Castro, B., Farina, C., Freeman, M., Gallo, V., Goldman, J.E., Goldman, S.A., Götz, M., Gutiérrez, A., Haydon, P.G., Heiland, D.H., Hol, E.M., Holt, M.G., Iino, M., Kastanenka, K.V., Kettenmann, H., Khakh, B.S., Koizumi, S., Lee, C.J., Liddelow, S.A., MacVicar, B.A., Magistretti, P., Messing, A., Mishra, A., Molofsky, A.V., Murai, K.K., Norris, C.M., Okada, S., Oliet, S.H.R., Oliveira, J.F., Panatier, A., Parpura, V., Pekna, M., Pekny, M., Pellerin, L., Perea, G., Pérez-Nievas, B.G., Pfrieger, F.W., Poskanzer, K.E., Quintana, F.J., Ransohoff, R.M., Riquelme-Perez, M., Robel, S., Rose, C.R., Rothstein, J.D., Rouach, N., Rowitch, D.H., Semyanov, A., Sirko, S., Sontheimer, H., Swanson, R.A., Vitorica, J., Wanner, I.B., Wood, L.B., Wu, J., Zheng, B., Zimmer, E. R., Zorec, R., Sofroniew, M.V., Verkhratsky, A., 2021. Reactive astrocyte nomenclature, definitions, and future directions. Nat. Neurosci. 24, 312–325. https://doi.org/10.1038/S41593-020-00783-4.

Familian, A., Eikelenboom, P., Veerhuis, R., 2007. Minocycline does not affect amyloid β phagocytosis by human microglial cells. Neurosci. Lett. 416, 87–91. https://doi.org/10.1016/j.neulet.2007.01.052.

Farhy-Tselnicker, I., Allen, N.J., 2018. Astrocytes, neurons, synapses: a tripartite view on cortical circuit development. Neural Dev. 13, 7. https://doi.org/10.1186/S13064-018-0104-Y.

Franceschi, C., Campisi, J., 2014. Chronic inflammation (Inflammaging) and its potential contribution to Age-Associated diseases. Biol. Sci. Cite J. J. Gerontol. A Biol. Sci. Med Sci. 69, S4–9. https://doi.org/10.1093/gerona/glu057.

Franceschi, C., Garagnani, P., Morsiani, C., Conte, M., Santoro, A., Grignolio, A., Monti, D., Capri, M., Salvioli, S., 2018. The continuum of aging and Age-Related diseases: common mechanisms but different rates. Front. Med. 5, 61. https://doi.org/10.3389/FMED.2018.00061.

Gaikwad, S., Puangmalai, N., Bittar, A., Montalbano, M., Garcia, S., McAllen, S., Bhatt, N., Sonawane, M., Sengupta, U., Kayed, R., 2018. Tau oligomer induced HMGB1 release contributes to cellular senescence and neuropathology linked to Alzheimer’s disease and frontotemporal dementia sagar. Physiol. Behav. 176, 139–148. https://doi.org/10.1016/j.celrep.2021.109419.Tau.

González-Gualda, E., Baker, A.G., Fruk, L., Muñoz-Espín, D., 2021. A guide to assessing cellular senescence in vitro and in vivo. FEBS J. 288, 56–80. https://doi.org/10.1111/FEBS.15570.

Griffin, K., Bejoy, J., Song, L., Hua, T., Marzano, M., Jeske, R., Sang, Q.X.A., Li, Y., 2020. Human stem Cell-derived aggregates of forebrain astroglia respond to amyloid beta oligomers. Tissue Eng. Part A 26, 527–542. https://doi.org/10.1089/ten.tea.2019.0227.

Guerrero, A., De Strooper, B., Arancibia-Cárcamo, I.L., 2021. Cellular senescence at the crossroads of inflammation and Alzheimer’s disease. Trends Neurosci. 44, 714–727. https://doi.org/10.1016/j.tins.2021.06.007.

Habib, N., McCabe, C., Medina, S., Varshavsky, M., Kitsberg, D., Dvir-Szternfeld, R., Green, G., Dionne, D., Nguyen, L., Marshall, J.L., Chen, F., Zhang, F., Kaplan, T., Regev, A., Schwartz, M., 2020. Disease-associated astrocytes in Alzheimer’s disease and aging. Nat. Neurosci. 23, 701–706. https://doi.org/10.1038/S41593-020-0624-8.

Han, X., Lei, Q., Liu, H., Zhang, T., Gou, X., 2024. SerpinA3N regulates the secretory phenotype of mouse senescent astrocytes contributing to neurodegeneration. J. Gerontol. Ser. A Biol. Sci. Med. Sci. 79, 1–9. https://doi.org/10.1093/gerona/glad278.

Han, X., Zhang, T., Liu, H., Mi, Y., Gou, X., 2020. Astrocyte senescence and Alzheimer's disease: a review. Front. Aging Neurosci. https://doi.org/10.3389/fnagi.2020.00148.
He, S., Sharpless, N.E., 2017. Senescence in health and disease. Cell 169, 1000–1011. https://doi.org/10.1016/j.cell.2017.05.015.
Hong, W., Hu, C., Wang, C., Zhu, B., Tian, M., Qin, H., 2023. Effects of amyloid β (Aβ)42 and gasdermin d on the progression of Alzheimer's disease in vitro and in vivo through the regulation of astrocyte pyroptosis. Aging 15, 12209–12224. https://doi.org/10.18632/aging.205174.
Huber, A.K., Giles, D.A., Segal, B.M., Irani, D.N., 2018. An emerging role for eotaxins in neurodegenerative disease. Clin. Immunol. 189, 29–33. https://doi.org/10.1016/j.clim.2016.09.010.
Hudson, H.R., Sun, X., Orr, M.E., 2025. Senescent brain cell types in Alzheimer's disease: pathological mechanisms and therapeutic opportunities. Neurotherapeutics 22, e00519. https://doi.org/10.1016/j.neurot.2024.e00519.
Jiang, M., Chen, G., 2009. Ca2+ regulation of dynamin-independent endocytosis in cortical astrocytes. J. Neurosci. 29, 8063–8074. https://doi.org/10.1523/JNEUROSCI.6139-08.2009.
Kawano, H., Oyabu, K., Yamamoto, H., Eto, K., Adaniya, Y., Kubota, K., Watanabe, T., Hirano-Iwata, A., Nabekura, J., Katsurabayashi, S., Iwasaki, K., 2017. Astrocytes with previous chronic exposure to amyloid β-peptide fragment 1–40 suppress excitatory synaptic transmission. J. Neurochem. 143, 624–634. https://doi.org/10.1111/jnc.14247.
Kayed, R., Head, E., Thompson, J.L., McIntire, T.M., Milton, S.C., Cotman, C.W., Glabel, C.G., 2003. Common structure of soluble amyloid oligomers implies common mechanism of pathogenesis. Science 300 (80), 486–489. https://doi.org/10.1126/SCIENCE.1079469/SUPPL_FILE/KAYED.SOM.PDF.
Keller, J.N., Hanni, K.B., Markesbery, W.R., 2000. Impaired proteasome function in Alzheimer's disease. J. Neurochem. 75, 436–439. https://doi.org/10.1046/j.1471-4159.2000.0750436.x.
Kelly, P., Sanchez-Mico, M.V., Hou, S.S., Whiteman, S., Russ, A., Hudry, E., Arbel-Ornath, M., Greenberg, S.M., Bacskai, B.J., 2023. Neuronally derived soluble abeta evokes Cell-Wide astrocytic calcium dysregulation in absence of amyloid plaques in vivo. J. Neurosci. 43, 4926. https://doi.org/10.1523/JNEUROSCI.1988-22.2023.
Koran, M.E.I., Wagener, M., Hohman, T.J., 2017. Sex differences in the association between AD biomarkers and cognitive decline. Brain Imaging Behav. 11, 205–213. https://doi.org/10.1007/s11682-016-9523-8.
Kovalevich, J., Langford, D., 2013. Considerations for the use of SH-SY5Y neuroblastoma cells in neurobiology. Methods Mol. Biol. 1078, 9–21. https://doi.org/10.1007/978-1-62703-640-5.
Kuchibhotla, K.V., Goldman, S.T., Lattarulo, C.R., Wu, H., Bradley, T., Bacskai, B.J., 2009. Aβ plaques lead to aberrant regulation of calcium homeostasis in vivo resulting in structural and functional disruption of neuronal networks. Neuron 59, 214–225. https://doi.org/10.1016/j.neuron.2008.06.008.A.
Lane, C.A., Hardy, J., Schott, J.M., 2018. Alzheimer's disease. Eur. J. Neurol. 25, 59–70. https://doi.org/10.1111/ene.13439.
Lazic, A., Balint, V., Ninkovic, D.S., Peric, M., Stevanovic, M., 2022. Reactive and senescent astroglial phenotypes as hallmarks of brain pathologies. Int. J. Mol. Sci. 23, 4995. https://doi.org/10.3390/IJMS23094995.
Liddelow, S.A., Barres, B.A., 2017. Reactive astrocytes: production, function, and therapeutic potential. Immunity 46, 957–967. https://doi.org/10.1016/J.IMMUNI.2017.06.006.
Limbad, C., Oron, T.R., Alimirah, F., Davalos, A.R., Tracy, T.E., Gan, L., Desprez, P.-Y., Campisi, J., 2020. Astrocyte senescence promotes glutamate toxicity in cortical neurons. PLoS One 15, e0227887. https://doi.org/10.1371/journal.pone.0227887.
Liu, M., Hurn, P.D., Roselli, C.E., Alkayed, N.J., 2007. Role of P450 aromatase in sex-specific astrocytic cell death. J. Cereb. Blood Flow. Metab. 27, 135–141. https://doi.org/10.1038/sj.jcbfm.9600331.
López-Otín, C., Blasco, M.A., Partridge, L., Serrano, M., Kroemer, G., 2022. Hallmarks of aging: an expanding universe. Cell S00928674 013770. https://doi.org/10.1016/j.cell.2022.11.001.
López-Teros, M., Alarcón-Aguilar, A., Castillo-Aragón, A., Königsberg, M., Luna-López, A., 2024. Cytokine profiling in senescent and reactive astrocytes: a systematic review. Neurobiol. Aging 138, 28–35. https://doi.org/10.1016/j.neurobiolaging.2024.02.012.
Loram, L.C., Sholar, P.W., Taylor, F.R., Wiesler, J.L., Babb, J.A., Strand, K.A., Berkelhammer, D., Day, H.E.W., Maier, S.F., Watkins, L.R., 2012. Sex and estradiol influence glial pro-inflammatory responses to lipopolysaccharide in rats. Psychoneuroendocrinology 37, 1688–1699. https://doi.org/10.1016/j.psyneuen.2012.02.018.
Lye, J.J., Latorre, E., Lee, B.P., Bandinelli, S., Holley, J.E., Gutowski, N.J., Ferrucci, L., Harries, L.W., 2019. Astrocyte senescence May drive alterations in GFAPα, CDKN2A p14 ARF, and TAU3 transcript expression and contribute to cognitive decline. GeroScience 41, 561–573. https://doi.org/10.1007/s11357-019-00100-3.
Maciel-Barón, L.Á., Morales-Rosales, S.L., Silva-Palacios, A., Rodríguez-Barrera, R.H., García-Álvarez, J.A., Luna-López, A., Pérez, V.I., Torres, C., Königsberg, M., 2018. The secretory phenotype of senescent astrocytes isolated from wistar newborn rats changes with anti-inflammatory drugs, but does not have a short-term effect on neuronal mitochondrial potential. Biogerontology 19, 415–433. https://doi.org/10.1007/s10522-018-9767-3.
Matias, I., Diniz, L.P., Damico, I.V., Araujo, A.P.B., Neves, L., da, Vargas, S., Leite, G., Suemoto, R.E.P., Nitrini, C.K., Jacob-Filho, R., Grinberg, W., Hol, L.T., Middeldorp, E.M., Gomes, J., F.C.A, 2022. Loss of lamin-B1 and defective nuclear morphology are hallmarks of astrocyte senescence in vitro and in the aging human hippocampus. Aging Cell 21, 1–18. https://doi.org/10.1111/acel.13521.
Montoliu-Gaya, L., Mulder, S.D., Veerhuis, R., Villegas, S., 2017. Effects of an Aβ-antibody fragment on Aβ aggregation and astrocytic uptake are modulated by apolipoprotein e and j mimetic peptides. PLoS One 12, 1–18. https://doi.org/10.1371/journal.pone.0188191.
Mun, B.-R., Park, S., Choi, W.-S., 2024. The oligomeric form of amyloid beta triggers astrocyte activation, independent of neurons. Chonnam Med. J. 60, 27. https://doi.org/10.4068/cmj.2024.60.1.27.
Narayan, P., Holmström, K.M., Kim, D.H., Whitcomb, D.J., Wilson, M.R., St. George-Hyslop, P., Wood, N.W., Dobson, C.M., Cho, K., Abramov, A.Y., Klenerman, D., 2014. Rare individual amyloid-β oligomers act on astrocytes to initiate neuronal damage. Biochemistry 53, 2442–2453. https://doi.org/10.1021/bi401606f.
Nielsen, H.M., Mulder, S.D., Beliën, J.A.M., Musters, R.J.P., Eikelenboom, P., Veerhuis, R., 2010. Astrocytic Aβ1-42 uptake is determined by Aβ-aggregation state and the presence of amyloid-associated proteins. Glia 58, 1235–1246. https://doi.org/10.1002/glia.21004.
Nielsen, H.M., Veerhuis, R., Holmqvist, B., Janciauskiene, S., 2009. Binding and uptake of Aβ1-42 by primary human astrocytes in vitro. Glia 57, 978–988. https://doi.org/10.1002/glia.20822.
Ortiz-sanz, C., Llavero, F., Zuazo-ibarra, J., Balantzategi, U., Quintela-lópez, T., Wyssenbach, A., Capetillo-zarate, E., Matute, C., Alberdi, E., Zugaza, J.L., 2022. Recombinant integrin β1 signal peptide blocks gliosis induced by Aβ oligomers. Int. J. Mol. Sci. 23. https://doi.org/10.3390/ijms23105747.
Osborn, L.M., Kamphuis, W., Wadman, W.J., Hol, E.M., 2016. Astrogliosis: an integral player in the pathogenesis of Alzheimer's disease. Prog. Neurobiol. 144, 121–141. https://doi.org/10.1016/j.pneurobio.2016.01.001.
Oseki, K.T., Monteforte, P.T., Pereira, G.J.S., Hirata, H., Ureshino, R.P., Bincoletto, C., Hsu, Y.T., Smaili, S.S., 2014. Apoptosis induced by Aβ25-35 peptide is Ca2+-IP3 signaling-dependent in murine astrocytes. Eur. J. Neurosci. 40, 2471–2478. https://doi.org/10.1111/ejn.12599.
Ostan, R., Bucci, L., Capri, M., Salvioli, S., Scurti, M., Pini, E., Monti, D., Franceschi, C., 2008. Immunosenescence and immunogenetics of human longevity. Neuroimmunomodulation 15, 224–240. https://doi.org/10.1159/000156466.
Ostan, R., Monti, D., Gueresi, P., Bussolotto, M., Franceschi, C., Baggio, G., 2016. Gender, aging and longevity in humans: an update of an intriguing/neglected scenario paving the way to a gender-specific Medicine. Clin. Sci. 130, 1711–1725. https://doi.org/10.1042/CS20160004.
Palmer, A.L., Ousman, S.S., 2018. Astrocytes and aging. Front. Aging Neurosci. 10, 337. https://doi.org/10.3389/FNAGI.2018.00337.
Pannuzzo, M., 2022. Beta-amyloid pore linked to controlled calcium influx into the cell: a new paradigm for Alzheimer's disease. Alzheimer'S. Dement. 18, 191–196. https://doi.org/10.1002/alz.12373.
Pekny, M., Pekna, M., 2014. Astrocyte reactivity and reactive astrogliosis: costs and benefits. Physiol. Rev. 94, 1077–1098. https://doi.org/10.1152/PHYSREV.00041.2013/ASSET/IMAGES/LARGE/Z9J0041427070009.JPEG.
Pekny, M., Wilhelmsson, U., Pekna, M., 2014. The dual role of astrocyte activation and reactive gliosis. Neurosci. Lett. 565, 30–38. https://doi.org/10.1016/J.NEULET.2013.12.071.
Pertusa, M., García-Matas, S., Rodríguez-Farré, E., Sanfeliu, C., Cristòfol, R., 2007. Astrocytes aged in vitro show a decreased neuroprotective capacity. J. Neurochem. 101, 794–805. https://doi.org/10.1111/j.1471-4159.2006.04369.x.
Pickering, A.M., Davies, K.J.A., 2012. Degradation of damaged proteins - the main function of the 20S proteasome. Prog. Mol. Biol. Transl. Sci. 109, 227. https://doi.org/10.1016/B978-0-12-397863-9.00006-7.
Qiu, C., Kivipelto, M., Von Strauss, E., 2009. Epidemiology of Alzheimer's disease: occurrence, determinants, and strategies toward intervention. Dialog. Clin. Neurosci. 11, 111–128. https://doi.org/10.31887/dcns.2009.11.2/cqiu.
Querol-Vilaseca, M., Colom-Cadena, M., Pegueroles, J., Nuñez-Llaves, R., Luque-Cabecerans, J., Muñoz-Llahuna, L., Andilla, J., Belbin, O., Spires-Jones, T.L., Gelpi, E., Clarimon, J., Loza-Alvarez, P., Fortea, J., Lleó, A., 2019. Nanoscale structure of amyloid-β plaques in Alzheimer's disease. Sci. Rep. 9, 1–10. https://doi.org/10.1038/s41598-019-41443-3.
Rabin, J.S., Lim, Y.Y., Papp, K.V., Jacobs, H.I.L., 2019. Sex, amyloid, and APOEε4 and risk of cognitive decline in preclinical Alzheimer's disease: findings from three well-characterized cohorts. Alzheimers Dement 14, 1193–1203. https://doi.org/10.1016/j.jalz.2018.04.010.Sex.
Rodier, F., Campisi, J., 2011. Four faces of cellular senescence. J. Cell Biol. https://doi.org/10.1083/jcb.201009094.
Rostami, J., Mothes, T., Kolahdouzan, M., Eriksson, O., Moslem, M., Bergström, J., Ingelsson, M., O'Callaghan, P., Healy, L.M., Falk, A., Erlandsson, A., 2021. Crosstalk between astrocytes and microglia results in increased degradation of α-synuclein and amyloid-β aggregates. J. Neuroinflamm. 18, 1–20. https://doi.org/10.1186/s12974-021-02158-3.
Salvioli, S., Ardizzoni, A., Franceschi, C., Cossarizza, A., 1997. JC-1, but not DiOC6(3) or rhodamine 123, is a reliable fluorescent probe to assess delta psi changes in intact cells implications for studies on mitochondrial functionally during apoptosis. FEBS Lett. 411, 77–82.
Santos-Galindo, M., Acaz-Fonseca, E., Bellini, M.J., Garcia-Segura, L.M., 2011. Sex differences in the inflammatory response of primary astrocytes to lipopolysaccharide. Biol. Sex. Differ. 2, 1–11. https://doi.org/10.1186/2042-6410-2-7.
Selkoe, D.J., Hardy, J., 2016. The amyloid hypothesis of Alzheimer's disease at 25 years. EMBO Mol. Med 8, 595–608. https://doi.org/10.15252/emmm.201606210.
Shafqat, A., Khan, S., Omer, M.H., Niaz, M., Albalkhi, I., AlKattan, K., Yaqinuddin, A., Tchkonia, T., Kirkland, J.L., Hashmi, S.K., 2023. Cellular senescence in brain aging and cognitive decline. Front. Aging Neurosci. 15, 1281581. https://doi.org/10.3389/fnagi.2023.1281581.

Sheppard, O., Coleman, M., 2020. Alzheimer's disease: etiology, neuropathology and pathogenesis. Alzheimer'S. Dis. Drug Discov. 1–22. https://doi.org/10.36255/EXONPUBLICATIONS.ALZHEIMERSDISEASE.2020.CH1.

Shrivastava, A.N., Kowalewski, J.M., Renner, M., Bousset, L., Koulakoff, A., Melki, R., Giaume, C., Triller, A., 2013. β-amyloid and ATP-induced diffusional trapping of astrocyte and neuronal metabotropic glutamate type-5 receptors. Glia 61, 1673–1686. https://doi.org/10.1002/GLIA.22548.

Simmnacher, K., Krach, F., Schneider, Y., Alecu, J.E., Mautner, L., Klein, P., Roybon, L., Prots, I., Xiang, W., Winner, B., 2020. Unique signatures of stress-induced senescent human astrocytes. Exp. Neurol. 334, 113466. https://doi.org/10.1016/j.expneurol.2020.113466.

Sofroniew, M.V., 2015. Astrocyte barriers to neurotoxic inflammation. Nat. Rev. Neurosci. 16, 249–263. https://doi.org/10.1038/NRN3898.

Sofroniew, M.V., Vinters, H.V., 2010. Astrocytes: biology and pathology. Acta Neuropathol. 119, 7–35. https://doi.org/10.1007/s00401-009-0619-8.

Söllvander, S., Nikitidou, E., Brolin, R., Söderberg, L., Sehlin, D., Lannfelt, L., Erlandsson, A., 2016. Accumulation of amyloid-β by astrocytes result in enlarged endosomes and microvesicle-induced apoptosis of neurons. Mol. Neurodegener. 11, 38. https://doi.org/10.1186/S13024-016-0098-Z.

Söllvander, S., Nikitidou, E., Gallasch, L., Zyśk, M., Söderberg, L., Sehlin, D., Lannfelt, L., Erlandsson, A., 2018. The Aβ protofibril selective antibody mAb158 prevents accumulation of Aβ in astrocytes and rescues neurons from Aβ-induced cell death. J. Neuroinflamm. 15, 1–15. https://doi.org/10.1186/s12974-018-1134-4.

Stine, W.B., Dahlgren, K.N., Krafft, G.A., LaDu, M.J., 2003. In vitro characterization of conditions for Amyloid-β peptide oligomerization and fibrillogenesis. J. Biol. Chem. 278, 11612–11622. https://doi.org/10.1074/JBC.M210207200.

Tseng, B.P., Green, K.N., Chan, J.L., Blurton-Jones, M., LaFerla, F.M., 2008. Aβ inhibits the proteasome and enhances amyloid and tau accumulation. Neurobiol. Aging 29, 1607–1618. https://doi.org/10.1016/J.NEUROBIOLAGING.2007.04.014.

Turnquist, C., Horikawa, I., Foran, E., Major, E.O., Vojtesek, B., Lane, D.P., Lu, X., Harris, B.T., Harris, C.C., 2016. p53 isoforms regulate astrocyte-mediated neuroprotection and neurodegeneration. Cell Death Differ. 23, 1515–1528. https://doi.org/10.1038/cdd.2016.37.

Tuzer, F., Torres, C., 2022. Involvement of astrocyte senescence in Alzheimer's disease. Curr. Opin. Neurobiol. 76, 102594. https://doi.org/10.1016/j.conb.2022.102594.

Ungerleider, K., Beck, J.A., Lissa, D., Joruiz, S., Horikawa, I., Harris, C.C., 2022. Δ133p53α protects human astrocytes from Amyloid-Beta induced senescence and neurotoxicity. Neuroscience 498, 190–202. https://doi.org/10.1016/J.NEUROSCIENCE.2022.06.004.

Wyssenbach, A., Quintela, T., Llavero, F., Zugaza, J.L., Matute, C., Alberdi, E., 2016. Amyloid β-induced astrogliosis is mediated by β1-integrin via NADPH oxidase 2 in Alzheimer's disease. Aging Cell 15, 1140–1152. https://doi.org/10.1111/acel.12521.

Yslas, A.R., Park, R., Nishimura, N., Lee, E., 2024. Monomeric and oligomeric amyloid-β cause distinct Alzheimer's disease pathophysiological characteristics in astrocytes in human glymphatics-on-chip models. Lab Chip 24, 3826–3839. https://doi.org/10.1039/d4lc00287c.

Zhang, H., Su, Y.J., Zhou, W.W., Wang, S.W., Xu, P.X., Yu, X.L., Liu, R.T., 2014. Activated scavenger receptor a promotes glial internalisation of Aβ. PLoS One 9, 1–11. https://doi.org/10.1371/journal.pone.0094197.

Zhang, W., Yang, X., Liu, J., Pan, Y., Zhang, M., Chen, L., 2022. Senescent phenotype of astrocytes leads to activation of BV2 microglia and N2a neuronal cells death. Molecules 27, 1–19. https://doi.org/10.3390/molecules27185925.

Zhao, X., Yang, J., 2010. Amyloid-B peptide is a substrate of the human 20S proteasome. ACS Chem. Neurosci. 1, 655–660. https://doi.org/10.1021/cn100067e.